Journal of South American Earth Sciences 86 (2018) 176–192

Contents lists available at ScienceDirect

Journal of South American Earth Sciences

journal homepage: www.elsevier.com/locate/jsames

Geochemical and detrital zircon geochronological investigation of the metavolcanosedimentary Araticum complex, sergipano fold belt: Implications for the evolution of the Borborema Province, NE Brazil

Haroldo Monteiro Lima[a,*], Márcio Martins Pimentel[a], Reinhardt A. Fuck[a], Lauro Cézar Montefalco de Lira Santos[b], Elton Luiz Dantas[a]

[a] Programa de Pós-graduação em Geologia, Universidade de Brasília, Campus Universitário Darcy Ribeiro ICC, Asa Norte, CEP 70919-970, Brasília, DF, Brazil
[b] Universidade Federal de Pernambuco, Departamento de Geologia, Av. da Arquitetura, Cidade Universitária, Recife, PE, Brazil

ARTICLE INFO

Keywords:
Neoproterozoic island arc
Cariris Velhos Orogeny
Borborema Province
Western Gondwana

ABSTRACT

The Borborema Province is an important Precambrian orogenic system in Northeastern Brazil. It was formed during the assembly of Western Gondwana in the Brasiliano-Pan-African Orogeny. The Neoproterozoic Sergipano Belt is part of the Province and occupies a large area of its southern portion. Investigation of provenance and tectonic environment of the metavolcanic-sedimentary complexes in this belt are of regional amplitude and may reveal important aspects of the evolution of the province. In this study new whole-rock geochemistry, isotope Nd data and U-Pb geochronological data on detrital zircon of the metavolcanic-sedimentary Araticum Complex within the northeastern part of the Sergipano Belt, in order to contribute to the understanding the role of the Sergipano Belt in amalgamation of Western Gondwana. The related data indicate provenance from eroded island arcs and back-arc-relate settings during the Neoproterozoic. Detrital zircon grains indicate populations of Ediacaran-Cryogenian (ca. 660-620 Ma) and Tonian-Stenian ages (around ca. 1047 Ma) suggesting that source areas represent extinct volcanic arcs of the Pernambuco-Alagoas Domain to the north. Based on this study, it is suggested that sediments of the Araticum paleobasin were deposited in an oceanic environment during the arc exhumation over the Brasiliano-Pan African Orogeny, but also with strong contributions from Stenian island arcs, which are attributed to the Cariris Velhos Orogeny. Our results support that major supracrustal sequences of the Sergipano Fold Belt were deposited in the Neoproterozoic, such as indicated by previous studies.

1. Introduction

The understanding of Precambrian supracrustal sequences demands integrated studies, including field work combined with isotope geochemistry and elemental geochemical tools which are instrumental to access tectonic and sedimentological parameters and to constrain the geological record of the precursor basins (McLennan et al., 1993; Cawood et al., 1999; Košler et al., 2002). Nd isotopic and geochemical data are useful to investigate the tectonic setting of the sediment sources (Gu et al., 2002; Košler et al., 2002).

The Borborema Province (BP) in NE Brazil comprises an important segment of Western Gondwana, being characterized by Neoproterozoic fold belts and a mosaic of terranes/domains, that are dominated by major supracrustal sequences, that are host rocks for numerous granitic intrusions, marking the final assembly of Western Gondwana (Brito Neves et al., 2000). Therefore, a major correlation with the Borborema Province and western African sequences records major continental deformation, metamorphic and tectonic events (e.g. Santos et al., 2004; Hollanda et al., 2015; Oliveira et al., 2015; Neves et al., 2009, 2017).

Several supracrustal sequences are exposed within the Sergipano Fold Belt. They have been strongly affected by transpressional tectonics related to the final oblique convergence of older domains of the Borborema and Benin-Nigeria provinces with the São Francisco-Congo Craton (Caby, 1989; D'el-Rey Silva, 1999; Brito Neves et al., 2002). In addition, major crustal shear zones limit such sequences and they may be correlated with the Yaoundé Fold Belt in the Cameroon, Africa (Oliveira et al., 2006, 2015; Mendes et al., 2011).

In Western Gondwana, little is known from the role of metasedimentary complexes in its mobile belts. In the BP, such sequences strongly vary in age, covering Paleoproterozoic migmatized sequences (Santos et al., 2004) and Neoproterozoic pelitic and psamitic units (Neves and Alcantara, 2010). However, the precise geochronological

* Corresponding author.
E-mail addresses: haroldogeologo@gmail.com (H.M. Lima), lauromontefalco@gmail.com (L.C.M.d.L. Santos).

https://doi.org/10.1016/j.jsames.2018.06.013
Received 20 November 2017; Received in revised form 13 June 2018; Accepted 18 June 2018
Available online 22 June 2018
0895-9811/

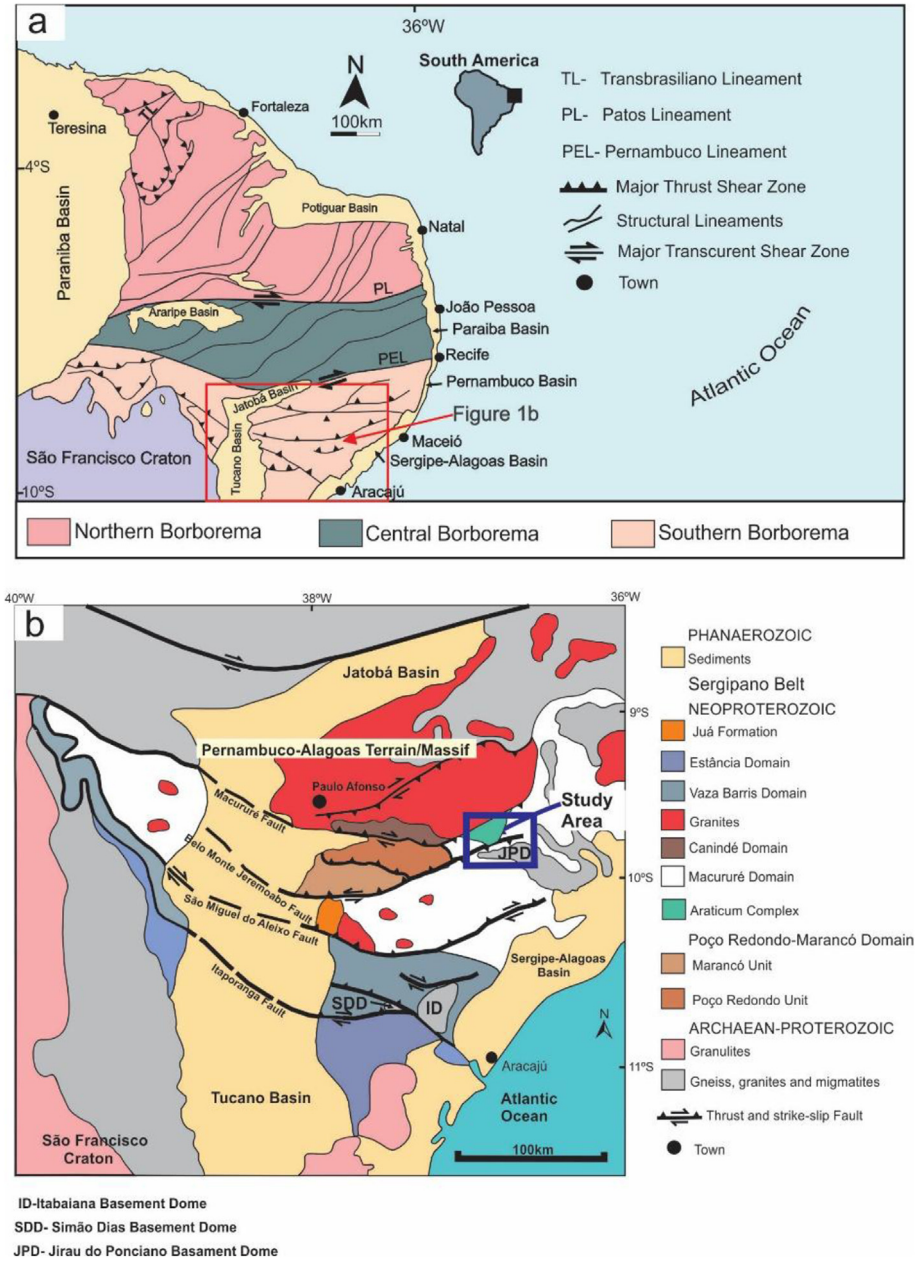

Fig. 1. a) Schematic geological map displaying the main tectonic units of the Borborema Province (modified from Brito Neves et al., 2000). b) General geologic context of the Sergipano Belt, with the study area highlighted by the blue open rectangle (modified from D'el-Rey Silva, 1999 and Oliveira et al., 2006). (For interpretation of the references to color in this figure legend, the reader is referred to the Web version of this article.)

and stratigraphic aspects of such rocks is still problematic, mainly due the influence of regional deformation. In this sense, our paper aims to investigate the nature and sources of metasedimentary and metavolcanic rocks of the Araticum Complex (ATC), which is one of the largest occurrences of metavolcanic-sedimentary sequences in the Sergipano Belt, as well as to suggest possible correlatives (i.e. Macururé or Marancó-Poço Redondo Domains, Carvalho, 2005; Oliveira et al., 2015), once that the origin of such rocks, including its major geotectonic related domains are still unknown.

The study is based on U-Pb detrital zircon dating combined with Nd systematics and whole-rock geochemistry. Our goals are: (i) to assess the depositional age of this sequence contributing to its stratigraphic significance, (ii) obtain information on its original tectonic setting and demonstrate the implications of our results for Sergipano Fold Belt evolution, specially based on the South America-Africa connection.

2. Geological setting

The Borborema Province comprises several Neoproterozoic fold belts, domain, massifs and terranes, that are limited my major shear zones Brito Neves et al., 2000; Van Schmus et al., 2008; Ganade de Araujo et al., 2014). It is widely accepted that the province resulted from the convergence between the Amazonian, São Luis-West Africa and São Francisco-Congo cratons during the Brasiliano-Pan African orogeny (Trompette, 1994; Van Schmus et al., 2008, 2011).

It is connected to Africa via several tectonic provinces, including the

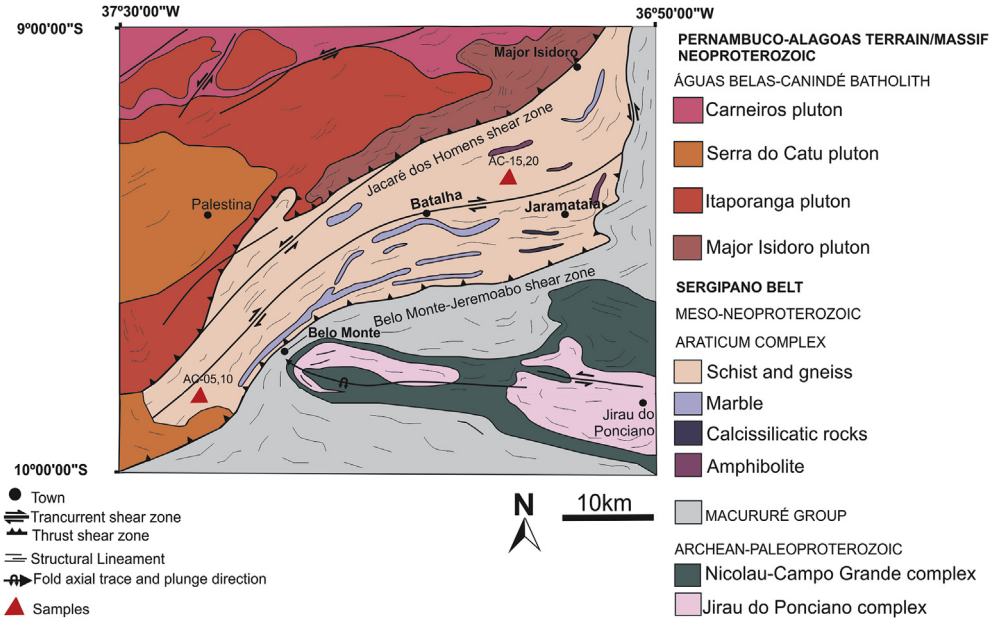

Fig. 2. Simplified geological map of the study area, emphasizing the Araticum metavolcanic-sedimentary Complex and location of two samples collected for U-Pb geochronology in detrital zircon.

Trans-Sahara, Benin-Nigeria, Oubanguides and Yaoundé (Caby, 1989; Castaing et al., 1993; Toteu et al., 2001; Brito Neves et al., 2002; Oliveira et al., 2006; Arthaud et al., 2008; Van Schmus et al., 2008). Several authors interpret its evolution as a polycyclic regime, involving accretionary processes developed during two orogenies: Cariris Velhos (920–1000 Ma) and Brasiliano/Pan-Africano (650-580 Ma, Santos, 1996; Brito Neves et al., 2000; Santos et al., 2010; Padilha et al., 2016; Santos et al., 2018a). In addition, recent papers from Santos et al. (2018b), Neves et al. (2015), among others, has also demonstrated a significant role of Paleoproterozoic and Archean crustal accretion.

The Patos and Pernambuco lineaments are the most expressive boundaries between domains, separating major subprovinces: Northern, Central and Southern (Van Schmus et al., 1995, Fig. 1a). The southern sub province is the area of interest of the present study. This is divided as follows: Pernambuco-Alagoas Terrane/Domain and Riacho do Pontal, Rio Preto and Sergipano fold belts (Brito Neves et al., 2000; Oliveira et al., 2010; Caxito and Uhlein, 2013; Caxito et al., 2016). The Sergipano Fold Belt (Fig. 1b) has a triangular shape, limited by the Pernambuco-Alagoas Terrane in the north (TPEAL) and the São Francisco Craton in the south (D'el-Rey Silva, 1999).

It is has been suggested that the origin of the Sergipano Fold Belt is related to the oblique collision between the Borborema-Benin-Nigeria-Cameroon provinces and the São Francisco-Congo paleoplate, during the late Neoproterozoic (D'el-Rey Silva et al., 2007; Silva et al., 2008). Some authors (e.g Trompette, 1994) suggested that the Sergipano Belt is connected with the Oubanguides Belt in West Africa (Toteu et al., 2001; Oliveira et al., 2006). The Sergipano Belt is divided into five distinct domains, which are limited by regional shear zones: Canindé, Poço Redondo-Marancó, Macururé, Vaza Barris and Estância domains (Davison and Santos, 1989; D'el-Rey Silva, 1999; Carvalho, 2005; Oliveira et al., 2010, 2015, Fig. 1b). Several metavolcanic-sedimentary sequences, including the ATC occur in the Macururé Domain (NE of the Sergipano Fold Belt), which are structurally controlled by transpression shear zones, and present variable geochemical characteristics (Mendes et al., 2009).

According to preliminary studies, these rocks seem to be in tectonic contact with granitic rocks of the Águas Belas-Canindé batholith in the Pernambuco-Alagoas Terrane through the transpressional Jacaré dos Homens Shear Zone, and in the south, it is limited by the Belo Monte-Jeremoabo Thrust Shear Zone (Fig. 1b, Medeiros, 2000; Brito et al., 2008; Mendes et al., 2009; Brito and Mendes, 2011).

3. Field relationships

The ATC is in contact, to the north, with the Águas Belas-Canindé Batholith of the Pernambuco-Alagoas Domain along the Jacaré dos Homens transpressional shear zone. The batholith comprises the Carneiros, Itaporanga, Serra do Catú and Major Isidoro plutons (Mendes et al., 2009). It comprises paragneisses, schists, and felsic to intermediate metavolcanic rocks, which are interlayered with amphibolites and marbles (Fig. 2).

Felsic to intermediate metavolcanic rocks occur as lenses affected by regional deformation, forming lenticular bodies of metavulcanoclastic rocks associated with metasedimentary rocks. The mafic metavolcanic rocks are represented by amphibolite lenses intercalated in the schists and paragneisses. Within the metasedimentary rocks, dark gray colored, fine to medium-grained sillimanite-garnet-muscovite-biotite schists with mm-sized garnet porphyroblasts, high obliquity lineation and low angle foliation are observed (Fig. 3a, c). Coarse-grained garnet-biotite paragneisses are banded and locally display folded quartz-feldspar lenses (Fig. 3b). They may be associated with metagraywacke.

The marbles are white to cream-colored, granoblastic texture, and may present muscovite and local incipient foliation (Fig. 3d). The diopside-bearing calc-silicate rocks are exposed as small lenses concordant with clastic metasedimentary rocks, and present fine to medium grain, light greenish color, (Fig. 3e). The mafic metavolcanic rocks are represented by amphibolite lenses associated with micaschists and paragneisses. The amphibolites show strong foliation formed by the orientation of medium-grained prismatic crystals. A discrete banded structure is also observed (Fig. 3f).

The garnet-biotite paragneisses have granoblastic texture and are composed of quartz, plagioclase, K-feldspar, biotite, garnet, titanite, apatite, zircon and opaque minerals. The quartz crystals have dimensions around 0.5–1 mm, are usually anhedral and deformed in the shear

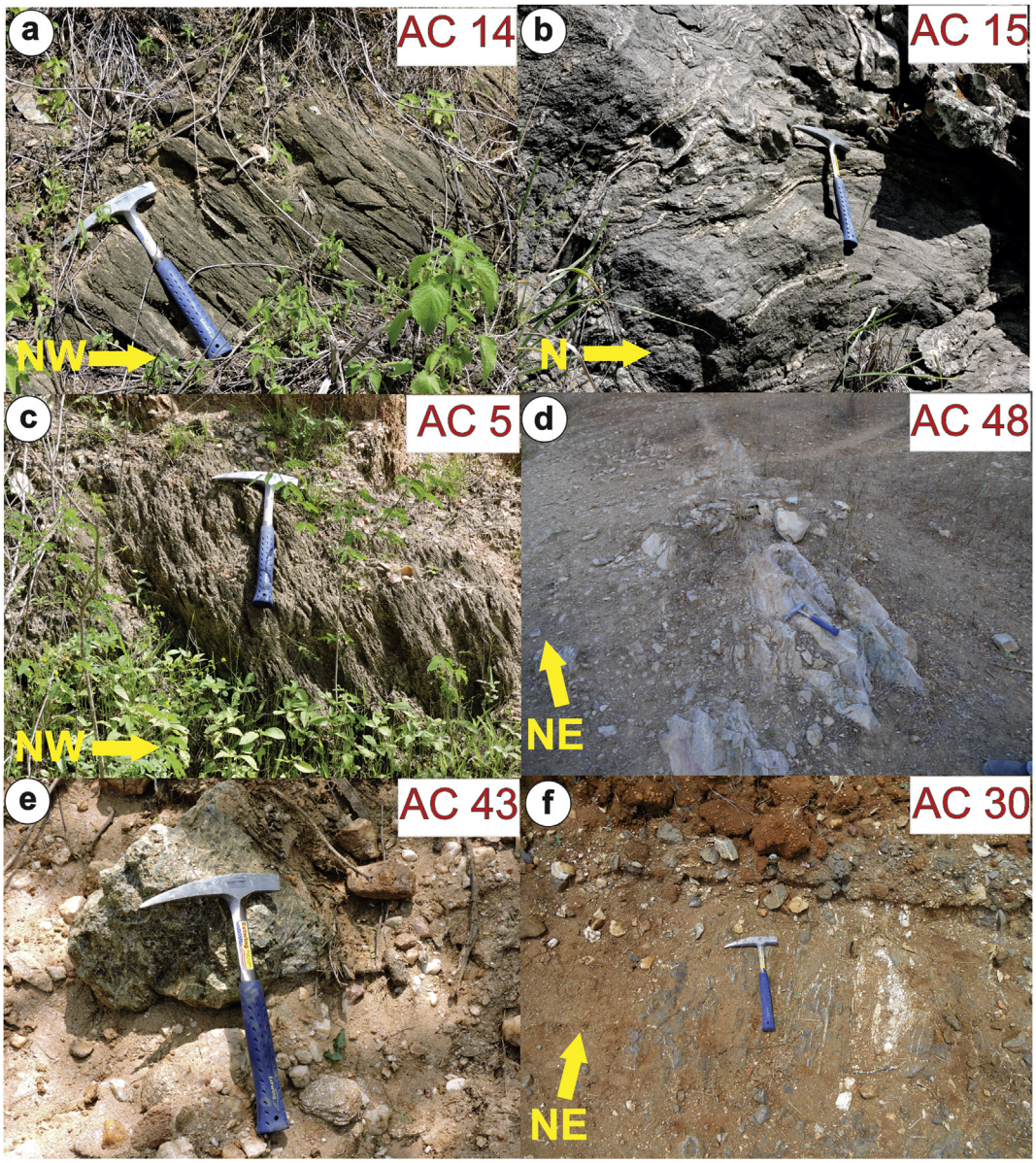

Fig. 3. Field features of the Araticum Complex. a) garnet-biotite gneiss quartzo-feldspar with 35° low angle foliation exhibiting tangential tectonics with dip to NW. b) biotite paragneisse with quartz-feldspar folded layers in the transpressional Jacaré dos Homens shear zone c) sillimanite-garnet-muscovite-biotite schist with high angle foliation 65°/NW. d) Marble lens concordant to the structure of the garnet-muscovite-biotite schists and biotite paragneiss of the Araticum Complex. e) Diopside-bearing calc-silicate rock lens. f) Lens of banded amphibolite (mafic metavolcanic rock) concordant with the metasedimentary rocks of the Araticum Complex.

zones presenting ribbons and dynamic recrystallization by migration of grain boundaries. Plagioclase has dimensions between 0.5 and 1 mm, is subhedral to anhedral and exhibits, in some rocks, low degree of saussuritization. K-feldspar has dimension of about 0.5 mm and is subhedral to anhedral, being represented by microcline and orthoclase. Biotite and muscovite occur as lamellae oriented in the sillimanite-garnet-muscovite-biotite schists and biotite paragneisses and are deformed by ductile regime.

Zircon occurs in significant amounts, dispersed in the matrix as well as in the biotite lamellae (Fig. 4a). The presence of sillimanite (fibrolite), was also observed in some sillimanite-garnet-muscovite-biotite schists (Fig. 4b). The garnet crystals have dimensions between 0.2 and 2 mm across and show signs of alteration to chlorite and iron oxides in the fractures. Garnet is a subhedral form with a porphyroblastic aspect and sometimes occurs surrounded by biotite lamellae (Fig. 4c and d). Amphibolites present nematoblastic texture conferred by hornblende and plagioclase crystals (Fig. 4e and f). The amphibolites can be subdivided into three groups: common amphibolites, diopside-bearing amphibolites and garnet-bearing amphibolites. Common amphibolites include hornblende, plagioclase, chlorite, epidote, titanite and opaque minerals. Epidote exhibit dimensions between 1 and 2 mm and titanite around 1 mm (Fig. 4e and f).

The diopside-bearing amphibolites are composed of hornblende, plagioclase, diopside, epidote, titanite, quartz and opaque minerals. Epidote is granular with dimensions of 1 mm and crystals of titanite are anhedral with dimensions of 0.5 mm. Diopside is anhedral with sizes

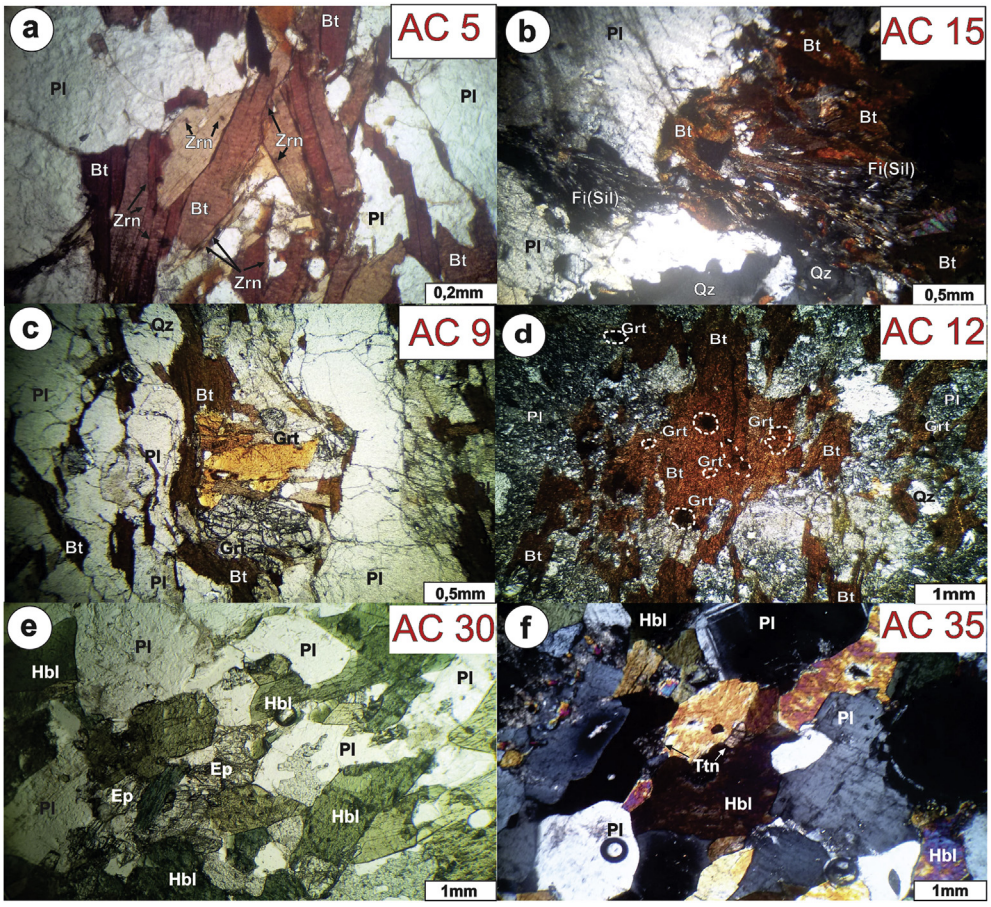

Fig. 4. Mineralogical and textural aspects of metavolcanic-sedimentary rocks of the Araticum Complex: a) Zircon grains included in biotite lamellae in micaschist. b) Lepidogranoblastic texture with sillimanite (fibrolite) generated from biotite in a quartz-feldspar matrix of the garnet-biotite paragneiss c) Porphyroclast of fractured garnet surrounded by lamellae of biotite in paragneiss. d) garnet grains included in biotite in metagraywacke. e) Nematogranoblastic texture and anhedral epidote crystals associated with hornblende in amphibolite. f) Plagioclase and titanite crystals on the hornblende border in ortho-derived amphibolite. Qz-quartz, Bt-biotite, Pl-plagioclase, Zrn-zircon, Fi (Sil)-fibrolite (sillimanite), Grt-garnet, Hbl-hornblende, Ep-epidote, Ttn-titanite.

between 1 and 3 mm and elongated along the main foliation. Garnet-bearing amphibolites are formed by hornblende, plagioclase, garnet, titanite and opaque minerals. Garnet crystals are anhedral, 1–2 mm in size, and are fractured with inclusions of opaque minerals.

4. Analytical procedures

Eighteen representative samples of metavolcanic-sedimentary rocks were selected for whole-rock geochemistry analysis in ALS Minerals laboratory. Major and trace elements were analyzed on ICP-AES with detection limit of 0.01% and ICP-MS with detection limit between 0.01 and 0.5 ppm after fusion using Li meta- and tetraborate and digestion with nitric acid. The average percentage of ignition loss in meta-volcanic-sedimentary rocks (LOI) is 2.29% and is determined by the difference in sample weight before and after heating at 1000 °C for 1 h.

Elements analyzed by ICP-AES include SiO_2, Al_2O_3, Fe_2O_3 (Total iron), CaO, MgO, Na_2O, K_2O, MnO and P_2O_5. ICP-MS was used to determine Ba, Ce, Cr, Cs, Dy, Er, Eu, Ga, Gd, Hf, Ho, La, Lu, Nb, Nd, Pr, Rb, Sm, Sn, Sr, Ta, Tb, Th, Tm, U, V, W, Y, Yb and Zr concentrations. Co, Cu, Li, Mo, Ni, Pb, Sc, and Zn concentrations were obtained by multi-acid digestion (four acids) and analyzed by ICP-AES with detection limits between 1 and 10 ppm (Tables 1 and 2). Data processing and diagrams construction were performed with the help of Petrograph software (Petrelli et al., 2005), Geochemical Data Toolkit (GCDKIT) and Excel sheets (Janousek et al., 2011). Sm-Nd isotopic analyses were performed on eighteen samples in the Geochronology laboratory of the University of Brasília following the procedure proposed by Gioia and Pimentel (2000, Table 3). Total rock samples (ca. 50 mg) were mixed with a combined ^{149}Sm-^{150}Nd spike solution and dissolved in Savillex capsules. Extraction of Sm and Nd from whole-rock samples followed conventional cation exchange techniques, using Teflon columns containing LN-Spec resin (HDEHP–diethylhexyl phosphoric acid supported on PTFE powder).

Sm and Nd samples were deposited on double Re filaments and isotopic measurements were performed on a Triton multicollector thermal ionization mass spectrometer, Thermo Scientific. Uncertainties in Sm/Nd and $^{143}Nd/^{144}Nd$ ratios are around 0.4% (1σ) and ± 0.005% (1σ), respectively, based on repeated analyses of BHVO-1 and BCR-1 international rock standards. $^{143}Nd/^{144}Nd$ was normalized to $^{146}Nd/^{144}Nd$ of 0.7219 and the decay constant (λ) used was 6.54×10^{-12}. T_{DM} models were calculated using DePaolo (1988) model.

U-Pb isotopic analysis of detrital zircon was limited for only two samples, and were performed at the Geochronology Laboratory of the University of Brasília. The main reason for this is the lack of good outcrop exposures, especially to fits with the necessary volume to concentrate zircon grains. The samples were initially crushed and sieved, and then the heavy minerals were separated using conventional gravimetric and magnetic methods. Zircon grains were separated using a binocular microscope and mounted on epoxy resin for isotopic determination by Laser Ablation Inductively Coupled Plasma Mass Spectrometry LA-MC-ICP-MS (Neptune). The mounts were imaged using backscatter electron (BS. The international standard GJ1 and substandard 91500 measured following the order of 1 blank, 1 sample and

Table 1
Major element (wt.%) concentrations of Araticum Complex. n.d.- not detected.

Sample	Garnet-biotite paragneisses and sillimanite-garnet-muscovite-biotite schists									Amphibolites								Marble		
	AC5	AC9	AC10	AC11	AC12	AC13	AC14	AC15	AC16	AC17	AC29	AC30	AC31	AC32	AC33	AC34	AC35	AC36	AC48	AC49	AC51
SiO_2	61.9	61.1	61.1	62.9	64.8	61.4	60.6	62.2	61.3	61.6	49.3	46.5	47	47.9	50.2	50.3	50	49.2	3.10	5.57	4.47
TiO_2	0.91	0.96	0.95	0.92	0.91	0.95	0.94	0.91	1.13	1.16	1.17	1.23	1.22	1.16	1.13	1.16	1.12	1.13	0.04	0.02	0.01
Al_2O_3	15.2	14.9	14.8	15.4	14.3	14.9	14.8	15.2	15.4	15.4	13.3	14.7	14.6	14.3	13.8	13.8	13.6	14.3	0.52	0.14	0.0
Fe_2O_3(total)	7.43	7.63	7.52	7.52	7.19	7.62	7.55	7.53	8.02	8.13	14.1	15.15	15.1	14.7	14.2	14.1	13.8	14.0	0.44	0.55	0.21
MnO	0.12	0.13	0.13	0.12	0.12	0.13	0.13	0.12	0.17	0.16	0.21	0.22	0.22	0.21	0.21	0.21	0.20	0.20	0.02	0.03	0.02
MgO	2.77	2.75	2.75	2.80	2.63	2.75	2.75	2.79	3.22	3.26	5.76	6.32	6.28	6.12	5.93	5.95	5.79	5.84	12.41	17.92	20.37
CaO	2.06	2.09	2.08	2.09	2.03	2.09	2.09	2.06	1.61	1.58	10.9	11.6	11.5	11.3	10.9	10.9	10.8	10.7	40.92	33.22	32.29
Na_2O	2.68	2.68	2.67	2.71	2.60	2.68	2.66	2.66	2.65	2.62	1.61	1.75	1.71	1.65	1.59	1.61	1.60	1.58	0.04	0.02	0.10
K_2O	2.72	2.76	2.74	2.75	2.66	2.76	2.75	2.75	3.23	3.25	0.30	0.35	0.35	0.33	0.32	0.33	0.30	0.33	0.01	0.04	0.02
P_2O_5	0.19	0.17	0.18	0.19	0.17	0.16	0.19	0.2	0.25	0.23	0.10	0.12	0.11	0.11	0.10	0.10	0.11	0.10	0.03	0.00	0.00
LOI	3.59	3.61	3.58	3.68	3.63	3.66	3.57	3.66	2.02	2.15	1.24	1.18	1.22	1.25	1.23	1.08	1.04	1.21	40.97	40.55	42.36
Total	99.5	98.7	98.5	101	101	99.1	98.1	100	99.0	99.5	98.0	99.1	99.3	99.0	99.6	99.6	98.5	98.6	98.5	98.0	99.8
K_2O/Na_2O	1.01	1.03	1.03	1.01	1.02	1.03	1.03	1.03	1.22	1.24	0.19	0.20	0.20	0.20	0.20	0.20	0.19	0.21			
SiO_2/Al_2O_3	4.06	4.10	4.11	4.08	4.53	4.11	4.09	4.08	3.97	3.99	3.71	3.15	3.21	3.35	3.64	3.64	3.66	3.44			
Fe_2O_3/K_2O	10.1	10.3	10.2	10.2	9.80	10.3	10.2	11.2	11.3	14.4	15.5	15.4	15.0	14.5	14.4	14.1	14.1	14.3			
CIA	59	58	58	58	57	57	58	59	60	60											
PIA	61	60	61	61	60	60	60	61	64	64											

CIA = $Al_2O_3/(Al_2O_3 + CaO^* + Na_2O + K_2O) \times 100$, molar ratio (Nesbitt and Young, 1982). CaO* corrected for Ca only in apatite.
PIA = $100 \times (Al_2O_3 - K_2O)/(Al_2O_3 + CaO + Na_2O - K_2O)$, molar ratio (Fedo et al., 1995).

1 standard were used (Jackson et al., 2004). These data were reduced on excel sheets following Bühn et al. (2009) and Chemale et al. (2012) and age calculations used Isoplot 4.15 (Ludwig, 2008).

5. Lithogeochemistry

5.1. Metasedimentary rocks

Whole-rock geochemistry of major, trace and rare earth elements give information on tectonic environment of paleobasins and provenance of sedimentary rocks (Bhatia, 1983; Armstrong-Altrin et al., 2004). Sillimanite-garnet-biotite schist and garnet-biotite paragneiss were selected because they were more abundant in the region. The analyzed rocks show intermediate concentrations of SiO_2 (61–65 wt%), high Al_2O_3 (14–15 wt%), K_2O (2.6–3.2 wt%) and SiO_2/Al_2O_3 ratios ranging between 3.9 and 4.5. Fe_2O_3/K_2O ratios range between 9.85 and 11.38. In order to quantify the weathering effect of metasedimentary rocks of the Araticum Complex, CIA and PIA indexes were used, since they show higher values with progressive weathering (Nesbitt and Young, 1982; Fedo et al., 1995). Plagioclase Index of Alteration -PIA (Al_2O_3-$K_2O/Al_2O_3 + CaO + Na_2O$-$K_2O$) varies from 50 for fresh rocks and close to 100 for clay minerals such as kaolinite, illite and gibbsite (Fedo et al., 1995).

Chemical Index of Alteration CIA ($Al_2O_3/(Al_2O_3 + CaO^* + Na_2O + K_2O)$*100 for the metasedimentary sequence of the Araticum Complex suggest that rocks in the source area suffered from mild or short-term chemical weathering. ($Al2O_3$-$K_2O/Al2O_3$ + CaO + Na_2O-K_2O) varies from 50 for fresh rocks and close to 100 for clay minerals such as kaolinite, illite and gibbsite (Fedo et al., 1995).

In the diagram TiO_2 vs. Fe_2O_{3T} + MgO proposed by Bhatia (1983, Fig. 5a) and used to discriminate tectonic environments, the ATC rocks are plotted exclusively in the field of oceanic islands. Similar behavior occurs in the log diagram (K_2O/Na_2O) vs. SiO_2 from Roser and Korsch (1986, Fig. 5b). Based on the content of SiO_2/Al_2O_3 vs. Log (K_2O/Na_2O), the samples indicate andesitic and basaltic sources from island arcs (Fig. 5c). Roser and Korsch (1988) proposed the use of discriminant functions in sedimentary rocks using major elements. In the F1 vs. F2 diagram of Roser and Korsch (1988), the samples studied here are distributed predominantly in the field of sources from felsic igneous rocks (Fig. 5d). ΣREE values (195–256, average 218) are compared to the global average for the ES (ΣREE = 230-European Shale, Haskin and Haskin, 1966) and PAAS (ΣREE = 212-Post-Archean Australian Shale, Table 4). REE diagram normalized for the North American Shale Composite-NASC, Haskin et al., 1966) shows subhorizontal spectrum with small fractionation of LREE relative to HREE (La_N/Yb_N = 1.22). Compared to the average upper continental crust (UCC, Rudnick and Gao, 2003) the samples show similar average pattern with (Eu/Eu* = 0.95), characteristic of post-archean sedimentary rocks (Fig. 5e). The spiderdiagram shows fractionation of Sr, Nb, U and enrichment of Rb, Th, La, Nd, La, Ce and Hf (Fig. 5f).

5.2. Amphibolites

These rocks exhibit SiO_2 contents between 46 and 50 wt% and low Al_2O_3 contents (13–14 wt%). High SiO_2 values, 50 wt% average, correspond to samples made of plagioclase, diopside and quartz. They have high CaO (11 wt%), medium MgO (6 wt%) contents and low K_2O (0.30 wt%). On the SiO_2 vs. Zr/TiO_2 (Winchester e Floyd,1977) diagram the amphibolites plot in the subalkaline basaltic field (Fig. 6a), whereas on the Th vs. Co diagram Hastie et al. (2007), suggested for altered and metamorphosed rocks, they share similarities with island arc tholeiitic to calc-alkaline basalts (Fig. 6b). The V vs. Ti/1000 diagram (Shervais, 1982) as well as the MnO - TiO_2 - P_2O_5 diagram of Mullen (1983), suggest that they correspond to island arc to back-arc related basalts (Fig. 6c and d). They can also be classified as iron-rich

Table 2
Trace element (ppm) concentrations of Araticum Complex. n.d.- not detected.

Sample	Garnet-biotite paragneisses and sillimanite-garnet-muscovite-biotite schists										Amphibolites							
	AC5	AC9	AC10	AC11	AC12	AC13	AC14	AC15	AC16	AC17	AC29	AC30	AC31	AC32	AC33	AC34	AC35	AC36
Sc	20	20	20	20	20	20	20	20	22	21	51	50	49	49	50	48	50	49
V	147	149	149	144	138	141	137	137	139	144	374	351	343	373	359	373	370	381
Cr	170	160	150	160	160	160	150	160	190	210	200	180	170	200	180	190	210	190
Co	19	20	20	20	20	19	20	20	38	24	43	43	42	41	42	42	42	42
Li	50	50	50	50	50	50	50	50	60	60	30	30	30	30	30	30	30	30
Mo	1	2	n.d.	1	1	2	2	n.d.	n.d.	n.d.	n.d.	n.d.	n.d.	1	1	1	1	n.d.
Ni	48	50	48	48	46	52	47	49	63	59	47	49	46	43	45	46	47	45
Cu	18	18	20	18	18	19	18	21	54	62	120	128	129	130	134	127	100	127
Zn	138	139	137	141	142	145	137	140	115	114	106	103	101	102	104	102	102	103
Ga	25	25.1	24.7	24.3	24.3	23.6	23.7	23.9	22.9	24.8	22.4	20.8	20.2	21.3	20.7	22	22	21.6
Rb	167.5	167.5	168.5	164	157.5	157.5	160	160.5	124.5	129	6.3	6	6	6.4	6.2	6.6	6.1	6.6
Sn	3	3	3	2	2	3	2	3	2	4	1	1	n.d.	1	1	1	1	1
W	6	6	4	5	6	6	4	5	5	8	8	6	4	4	4	5	6	4
Zr	201	213	209	198	208	210	213	208	286	307	61	57	54	64	58	61	61	60
Nb	15.1	17	15.7	15.1	14.7	14.3	21.4	15.6	17.4	18.2	1.4	1.5	1.2	1.6	1.5	1.6	1.7	1.4
Cs	7.38	7.65	7.38	7.09	7.18	6.96	7.09	7.12	8.24	8.65	0.19	0.15	0.17	0.21	0.18	0.2	0.14	0.2
Ba	821	833	822	769	772	774	784	791	575	592	128	115.5	112.5	121.5	117	127	140.5	118
La	37.9	41.7	37.4	38	38.1	37.3	35.2	44.2	44.8	42.1	4.7	4.5	4.4	4.7	4.6	4.8	4.7	4.8
Ce	73.8	81.1	71.8	73.2	71.2	72.2	67.9	83.9	89.6	83.2	11.5	11	10.4	11.1	10.6	11.5	11	11.3
Pr	8.35	9.01	8.12	8.45	8.17	8.19	7.55	9.51	10.45	9.73	1.65	1.53	1.52	1.6	1.52	1.59	1.56	1.57
Nd	33	34.2	30.4	32.3	30.8	31.4	28.6	35.6	39.1	37.1	8.4	7.6	7.3	7.8	7.8	8	7.7	8
Sm	6.65	6.82	5.97	6.13	5.94	6.02	6.06	6.78	7.73	7.37	2.7	2.48	2.23	2.53	2.35	2.56	2.5	2.47
Eu	1.29	1.28	1.28	1.37	1.4	1.34	1.33	1.34	1.52	1.56	0.98	0.9	0.95	0.81	0.89	0.97	0.99	1
Gd	5.75	5.97	5.93	5.98	6.05	5.67	5.99	6.79	7.48	7.52	3.79	3.66	3.85	3.62	4.08	3.86	3.67	3.71
Tb	0.81	0.91	0.86	0.89	0.87	0.79	0.89	0.93	1.16	1.14	0.67	0.63	0.63	0.63	0.63	0.61	0.69	0.66
Dy	5.08	5.17	4.98	5.06	5.08	5.08	4.85	5.43	6.44	6.67	4.18	4.3	3.94	4.05	4.17	3.81	4.2	4.23
Ho	1.02	1.06	1.05	1.08	1.04	0.95	1.13	1.14	1.42	1.31	0.96	1	0.92	0.92	0.93	0.9	1	0.92
Er	3.09	3.33	3.32	3.17	2.99	3.03	3.34	3.29	4.56	4.34	3.01	2.88	2.71	2.67	2.81	2.63	3.04	3.11
Tm	0.46	0.47	0.43	0.43	0.5	0.41	0.47	0.52	0.56	0.61	0.43	0.44	0.37	0.44	0.39	0.44	0.45	0.4
Yb	3.01	3.17	2.93	2.96	2.89	2.94	3.05	3.23	3.92	3.66	2.74	3.05	2.53	2.88	2.99	2.46	2.92	2.8
Lu	0.42	0.48	0.46	0.47	0.45	0.44	0.5	0.44	0.58	0.56	0.45	0.43	0.44	0.39	0.48	0.41	0.42	0.45
Y	27.6	29.8	29.2	27.5	27.4	26.6	28.2	29.1	36.5	37.3	26.2	24.7	23.5	26.3	25.8	26	25.9	25.4
Hf	5.8	6.2	6.1	5.9	6.4	6.4	6.3	6.2	8.7	9	1.8	1.9	1.6	1.7	1.6	1.6	1.9	1.8
Ta	0.9	0.9	0.9	0.8	0.9	0.8	1.4	1	1.1	1.1	n.d.	n.d.	n.d.	n.d.	n.d.	n.d.	n.d.	n.d.
Pb	19	20	17	16	19	18	22	20	48	18	n.d.	n.d.	3	5	3	n.d.	2	n.d.
Th	11.6	12.5	11.35	11.1	11.65	11	10.7	13.15	14.45	12.45	0.46	0.52	0.51	0.45	0.54	0.54	0.58	0.51
U	1.52	1.77	1.6	1.39	1.47	1.53	1.37	1.87	2.96	2.78	0.13	0.13	0.1	0.09	0.09	0.11	0.1	0.11
ΣREE	208	224	204	207	203	202	195	232	256	244	72	70	66	70	70	70.5	71	71
Eu/Eu*	0.90	0.88	0.94	0.99	1.02	1.01	0.97	0.87	0.92	0.88	0.94	0.91	0.98	0.82	0.87	0.94	1.00	1.01
$(La/Yb)_N$	1.22	1.27	1.24	1.24	1.28	1.23	1.12	1.33	1.22	1.27	1.23	1.06	1.25	1.17	1.10	1.40	1.15	1.23
$(La/Sm)_N$	1.02	1.09	1.12	1.10	1.14	1.10	1.03	1.16	1.02	1.09	1.12	1.17	1.27	1.20	1.26	1.21	1.21	1.25
$(Gd/Yb)_N$	1.14	1.12	1.20	1.20	1.25	1.15	1.17	1.25	1.14	1.12	1.14	0.99	1.26	1.04	1.13	1.30	1.04	1.10

$Eu/Eu^* = Eu_N/Eu^*$ $Eu^* = (Sm + Gd)_N/2$

tholeiites (Fig. 6e). Additionally, the ternary La/10-Y/15-Nb/8 diagram (Cabanis and Lecolle, 1989) suggests that these rocks correspond to tholeiite magmas generated in a compressive tectonic setting (Fig. 6f).

On the spiderdiagram normalized to the primitive mantle, the amphibolites show high contents of LILE and low HFSE. In general, the analyzed samples show strong similarities to the pattern of classic OIB and IAB magmas with depletion of Tb, Th, Nb and P and enrichment of Cs, Ba, K and Sr (Fig. 7a). Trace element contents of these rocks compared to the average values of OIB and IAB from Sun and McDonough (1989) and Dorendorf et al. (2000) indicate strong similarities with island arc basalts (IAB), with depleted Rb, Th, Nb and P and enriched Cs, Ba, K, Sr, Pb (Fig. 7a). Such pattern with depleted HFSE is generally interpreted as the result of mantle wedge melting in subduction environments, (Sun and McDonough, 1989; Ulmer, 2001). REE values normalized to chondrite are characterized by high La/Nb (2–3) and Zr/Y (average 2.3) ratios. These rocks show low LREE fractionation in relation to HREE (LaN/YbN = 1.1–1.2) displaying subhorizontal patterns. Eu/Eu* = 0.8–1 ratios suggest fractional crystallization of plagioclase (Fig. 7b).

6. Detrital zircon U-Pb geochronology

Two representative samples were selected for detrital zircon U-Pb analyses sillimanite-garnet muscovite-biotite schist (AC05) and garnet-biotite paragneisse (AC15). The results are in Table 4. BSE images and Th/U ratios define two major zircon populations: i) recrystallized angular to sub-angular micro fractured grains with low Th/U ratios (< 0.1), and ii) igneous prismatic grains with oscillatory zoning, with sizes varying between 50 and 100 μm and higher Th/U ratios > 0.2 (Fig. 8a and c). The morphology of zircon grains suggest that both populations represents metamorphic and igneous zircons with low reworking due to weathering. In general, such crystals are mostly fractured and exhibit patterns that reflects metamictization, indicating disorders in the Zr-O bonds, resulted from substitution of Zr by Th or U. In the most critical cases, concordance and quality of the data might be influenced by such features. The obtained ages for sample AC05 and AC15 ranges from Ediacaran to Cryogenian, with the younger grains around 597 Ma, being considered as the maximum age of deposition of the Araticum sequence (Fig. 8b, d). The most prominent peaks in the

Table 3
Sm-Nd isotopic data from Araticum Complex rocks.

Sample	Rock	Longitude (UTM zone 24S)	Latitude (UTM zone 24S)	Sm (ppm)	Nd (ppm)	$^{143}Nd/^{144}Nd$ (± 2SE)	$^{147}Sm/^{144}Nd$	ε(0)	εNd(600Ma)	εNd(900Ma)	T_{DM}(Ga)
AC01	Garnet-biotite paragneiss	−37.138326°	−9.689523°	8.856	43.370	0.512161(28)	0.1234	−9.30	−3.69	−0.89	1.48
AC04	Garnet-biotite paragneiss	−37.160100°	−9.696418°	10.658	54.609	0.512134(20)	0.1180	−9.84	−3.82	−0.81	1.44
AC05	Garnet-biotite paragneiss	−37.170631°	−9.723864°	9.989	56.226	0.511907(12)	0.1074	−14.25	−7.56	−4.14	1.62
AC09	Garnet-biotite paragneiss	−37.133119°	−9.668828°	8.848	29.819	0.511825(12)	0.1794	−15.85	−14.53	−13.86	1.85
AC10	Garnet-biotite paragneiss	−37.452655°	−9.665913°	8.143	42.060	0.512168(10)	0.1170	−9.16	−3.20	−0.15	1.37
AC11	Garnet-biotite paragneiss	−37.186053°	−9.648445°	8.047	37.900	0.512200(14)	0.1283	−8.55	6.72	9.34	1.49
AC14	Garnet-biotite paragneiss	−37.170099°	−9.581720°	6.835	33.985	0.512114(5)	0.1216	−10.23	7.27	10.14	1.52
AC15	sillimanite-garnet-muscovite-biotite schist	−37.208597°	−9.640680°	7.732	39.677	0.512128(5)	0.1178	−9.95	7.48	10.50	1.44
AC16	sillimanite-garnet-muscovite-biotite schist	−37.004512°	−9.707961°	6.607	33.299	0.512109(5)	0.1199	−10.32	7.39	10.33	1.51
AC17	sillimanite-garnet-muscovite-biotite schist	−37.189891°	−9.656530°	3.899	17.776	0.512187(7)	0.1326	−8.80	−3.89	−1.44	1.59
AC41	Calc-silicate rock	−37.212743°	−9.755842°	0.104	0.516	0.512257(12)	0.1218	−7.44	−1.70	1.17	1.29
AC42	Calc-silicate rock	−36.568763°	−9.8792152°	0.102	0.596	0.512347(89)	0.1036	−5.67	1.45	5.01	0.96
AC43	Calc-silicate rock	−36.556682°	−9.6825652°	0.107	0.516	0.512332(18)	0.1253	−5.96	−0.48	2.25	1.22
AC49	Marble	−37.133112°	−9.685119°	0.750	15.812	0.511090(49)	0,0287	−30.20	−17.34	−10.91	1.60
AC51	Marble	−37.244995°	−9.776948°	0.437	2.099	0.512077(10)	0,1259	−10.93	−5.52	−2.82	1.66
AC52	Marble	−37.658765°	−9.955468°	0.235	1.135	0.512102 (7)	0.1252	−10.45	−4.98	−2.25	1.60
AC53	Marble	−37.552584°	−9.189725°	0.435	2.159	0.512108 (12)	0.1219	−10.34	−4.60	−1.74	1.54
AC54	Marble	−37.002587°	−9.687952°	0.197	0.947	0.512109 (10)	0.125	−10.32	−4.82	−2.08	1.60
AC60	Garnet-biotite paragneiss	−37.023352°	−9.675937°	3.652	15.213	0.512227(9)	0,1451	−8.01	−4.07	−2.09	1.79
AC61	sillimanite-garnet-muscovite-biotite schist	−36.203012°	−9.773115°	3.471	15.088	0.512210 (7)	0.1391	−8.36	−3.94	−1.74	1.68
AC63	sillimanite-garnet-muscovite-biotite schist	−36.130468°	−9.711868°	5.144	23.840	0.512210(29)	0.1304	−8.34	−3.27	−0.74	1.51
AC64	sillimanite-garnet-muscovite-biotite schist	−36.561122°	−9.692320°	4.046	16.850	0.512226(11)	0.1452	−8.04	−4.10	−2.12	1.80
AC68	sillimanite-garnet-muscovite-biotite schist	−36.769400°	−9.675653°	3.770	16.070	0.512251(22)	0.1418	−7.56	−3.35	−1.25	1.66
AC29	amphibolite	−37.052233°	−9.732232°	3.068	9.143	0.512869 (7)	0.2028	4.51	4.04	3.80	–
AC30	amphibolite	−37.032211°	−9.554212°	3.266	10.077	0.512850 (9)	0.1959	4.14	4.19	4.22	–
AC31	amphibolite	−36.568820°	−9.688952°	2.775	8.414	0.521284(3)	0.1994	4.00	3.79	3.69	–
AC33	amphibolite	−36.86880°	−9.999875°	2.510	7.975	0.512866 (8)	0.1902	4.44	4.95	5.19	–

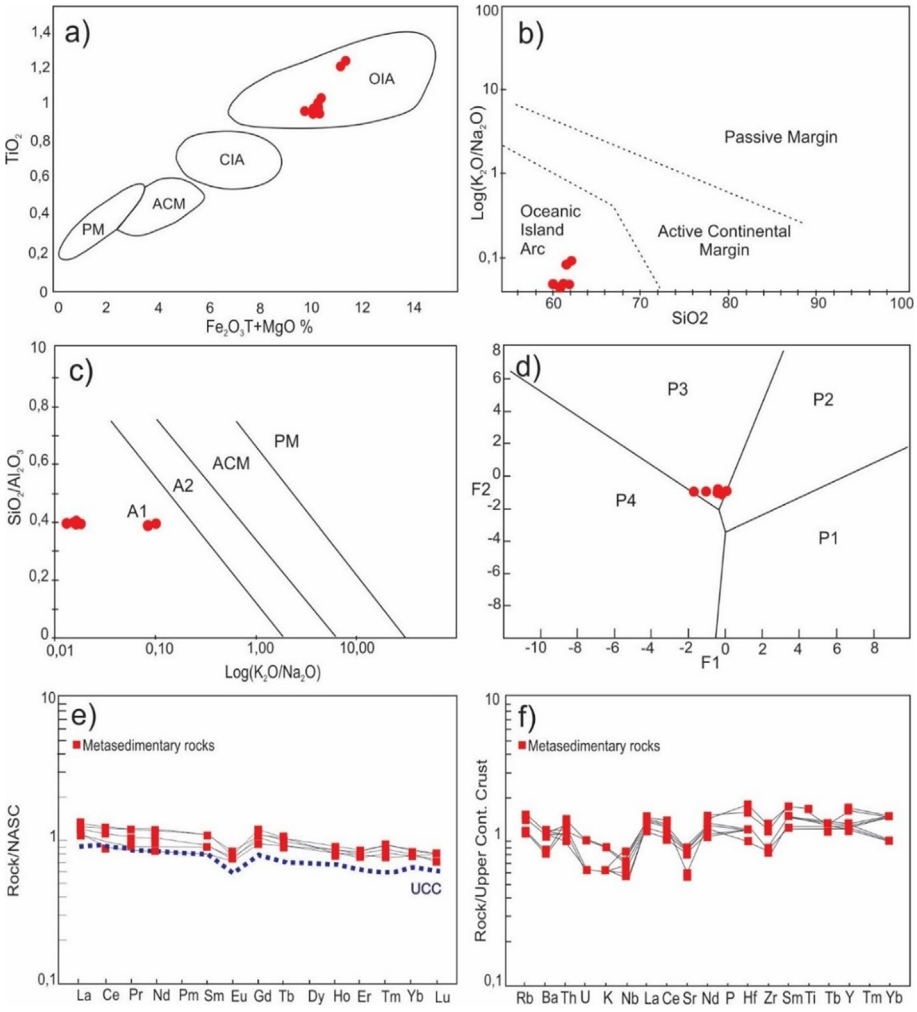

Fig. 5. Discriminant diagrams of tectonic environment (REE and multielement for sedimentary rocks of the Araticum Complex). a) Diagram of Bhatia (1983). b) Diagram of Roser and Korsch (1986). c) Diagram Maynard et al., 1982. d) Diagram of Roser and Korsch (1988). e) NASC-normalized REE diagram (North American Shale Composite, Haskin et al., 1966), UCC data from Rudnick and Gao (2003). f) UCC-normalized multielement diagram, data from Taylor and McLennan (1985). Abbreviations: OIA-oceanic island arc. CIA-continental island arc. ACM-active continental margins. PM-passive margins. A1-detritic sediments of andesitic and basaltic rocks deposited in oceanic island arcs. A2 - detritic sediments of felsic plutonic rocks deposited in oceanic island arcs. P1-provenance of mafic igneous rocks. P2-origin of intermediate igneous rocks. P3-origin of felsic igneous rocks. P4-provenance of quartz-rich sedimentary rocks.

frequency diagram are at 642 Ma and 1047 Ma (Fig. 8b). A minor amount of grains is Tonian-Stenian with a major peak at 1047 Ma. In addition, sample AC15 shows the majority of ages around 634 Ma, with a younger crystal with the age of 607 Ma (Fig. 8c and d) (see Table 5).

7. Nd isotopic composition

Sm-Nd analyses were performed on eighteen representative samples of metasedimentary and mafic metavolcanic rocks of the Araticum Complex.

Amphibolites intercalated in metasedimentary rocks exhibit $^{147}Sm/^{144}Nd$ ratios around 0.2 suggesting derivation from juvenile sources which may reflect the input from island arcs and back-arc which is also suggested by positive εNd (600Ma and 900Ma) values between 3.79 and 4.19 (Table 3).

Eight samples of garnet-biotite gneiss indicated T_{DM} ages between 1.37 and 1.85 and seven samples of sillimanite-garnet-muscovite-biotite schists with T_{DM} values between 1.44 and 1.80 as shown in Table 3. $^{147}Sm/^{144}Nd$ ratios fluctuate between 0.11 and 0.14. The spectrum of T_{DM} ages compared to other lithotectonic domains of the southern PB is shown in the histogram of Fig. 9. εNd (600Ma and 900Ma) parameter for metasedimentary rocks reflect the input immature nature source with juvenile contribution varying between negative and positive values −14.53 to 10.50.

Marbles samples (AC49 to AC54) intercalated in metasedimentary rocks indicated T_{DM} values between 1.60 and 1.66 Ga and a calc-silicate rock (AC21 to AC24) showed T_{DM} between 0.96 and 1.30 Ga.

8. Discussion

8.1. Geochemistry and source area weathering

The metasedimentary rocks show high values of SiO_2/Al_2O_3 and low K_2O/Na_2O (1–1.2) indicating presence of feldspar in the source rock. (Roser et al., 1996). All samples show low CaO (2 wt%) and TiO_2 (0.9 wt%). Al_2O_3/K_2O ratios are high with values ranging from 4.7 to 5.6 corroborating the high concentration of alumina-rich minerals also verified in the petrography. CIA and PIA indexes used as parameters to quantify the chemical weathering in the protolith (Nesbitt and Young, 1982, 1996; Fedo et al., 1995) show little chemical weathering and moderate presence of clay minerals in the source area.

The chemical alteration index (CIA) applied to metasedimentary rock of the Araticum Complex presents values between 57 and 60 and suggests that rocks from the source area underwent chemical weathering that was not severe since uplift and exposure in their present outcrops. In addition, PIA values ranging between 60 and 64 for these rocks indicate source area with significant presence of clay minerals.

Major and trace elements behavior on discriminant diagrams

Table 4
U–Pb detrital zircon ages extracted from sillimanite-garnet-muscovite-biotite schist of the Araticum Complex.

Atomic ratios Ages(Ma)												
AC5 Spot nº	$^{232}Th/^{238}U$	$^{207}Pb/^{206}Pb$	1σ (%)	$^{207}Pb/^{235}U$	1σ (%)	$^{206}Pb/^{238}U$	1σ (%)	$^{207}Pb/^{206}Pb$	1σ (%)	$^{207}Pb/^{235}U$	1σ (%)	Conc. (%)
070-ZR47	0.072	0.07130	0.97	1.747	1.27	1054	14	966	40	1026	16	109.1
065-ZR42	0.072	0.06236	0.51	0.917	0.94	653	9	686	22	661	9	95.2
063-ZR40	0.072	0.06242	3.51	0.853	4.39	609	30	688	146	626	41	88.5
060-ZR39	0.072	0.07435	2.83	1.367	3.68	807	35	1051	112	875	43	76.8
057-ZR36	0.072	0.07222	0.63	1.653	1.11	990	15	992	25	991	14	99.8
054-ZR33	0.072	0.06613	3.24	0.885	4.37	597	33	811	133	643	41	73.6
050-ZR32	0.799	0.07275	1.42	1.659	1.95	986	24	1007	57	993	25	97.9
048-ZR31N	0.392	0.07185	0.84	1.518	1.69	919	24	982	34	938	21	93.6
047-ZR30	0.845	0.07604	0.65	1.659	1.14	947	15	1096	26	993	14	86.4
046-ZR29	0.491	0.07310	0.89	1.646	1.36	975	17	1017	36	988	17	95.9
045-ZR28	0.007	0.06095	0.59	0.853	1.05	623	9	637	25	626	10	97.8
044-ZR27	0.271	0.07293	0.61	1.599	1.05	951	14	1012	25	970	13	94.0
043-ZR26	0.800	0.07823	1.10	1.502	1.55	840	16	1153	43	931	19	72.9
040-ZR25	0.008	0.06023	0.59	0.863	1.01	637	9	612	25	632	9	104.1
037-ZR22B	0.464	0.07288	0.47	1.668	0.86	990	11	1011	19	996	11	97.9
036-R22N	0.609	0.07265	0.80	1.653	1.35	984	17	1004	32	991	16	98.0
029-ZR18B	0.629	0.07374	1.04	1.692	1.06	992	14	1034	42	1006	17	95.9
024-ZR14B	0.003	0.06095	0.59	0.881	1.54	643	10	638	25	642	10	100.8
023-ZR14N	0.748	0.07373	1.03	1.512	3.34	894	18	1034	41	935	19	86.4
020-ZR13	0.209	0.06737	2.23	1.217	1.31	793	37	849	91	808	37	93.4
019-ZR12	0.004	0.06023	0.89	0.860	1.28	635	11	612	38	630	12	103.9
018-ZR11	0.502	0.07428	0.84	1.804	1.79	1046	17	1049	34	1047	17	99.7
016-ZR9	0.026	0.06087	0.89	0.873	3.91	638	18	635	38	637	17	100.5
015-ZR8	0.134	0.06890	1.93	1.005	1.09	648	42	896	79	706	39	72.3
014-ZR7	0.005	0.06099	0.58	0.867	1.21	633	10	639	25	634	10	99.0
013-ZR6	0.897	0.07855	0.73	1.763	2.83	972	16	1161	29	1032	16	83.8
010-ZR5	0.288	0.07643	1.99	1.740	0.90	985	36	1106	78	1023	36	89.0
007-ZR3	0.001	0.06136	0.40	0.887	1.97	643	9	652	17	645	9	98.6
006-ZR2	0.056	0.05972	1.50	0.807	1.35	603	14	594	64	601	18	99.5

suggest that the sedimentary sequence was deposited in an oceanic volcanic arc environment with material derived from erosion of andesitic and basaltic sources. REE contents in metasedimentary rocks of the Araticum Complex are similar to the ES (European Shale) and PASS (Post-Archean Australian Shale) and present slight LREE fractionation compared to HREE when normalized to the North American Shale Composite.

REE contents in metasedimentary rocks of the Araticum Complex are similar to the ES (European Shale) and PASS (Post-Archean Australian Shale) and present slight LREE fractionation compared to HREE when normalized to the North American Shale Composite.

Normalized trace elements with respect to UCC showed depletion in Sr, Nb and U and enrichment in Rb, La, Th Nd, Ce and Hf, suggesting weathering of feldspars generating a high content of clay minerals.

Amphibolites of the ATC, present chemical features similar to magmatic arc-related tholeiitic and calc-alkaline basalts. Also, our geochemical data suggest the influence of island arcs and back-arc basin components associated with the collision process (Fitton, 1971; Arculus, 2004). REE contents in the amphibolites (mafic metavolcanic rock) normalized to the chondrite show low fractionation of LREE in relation to HREE with subhorizontal pattern and very slight negative Eu anomaly, confirming the primitive origin of these rocks. Trace elements in amphibolites normalized with respect to the primitive mantle exhibit strong similarity with the pattern of oceanic volcanic arc basalts.

8.2. Detrital zircon U-Pb

Detrital zircon U-Pb analysis for LA-MC-ICP-MS from the metavolcanic-sedimentary Araticum Complex ranges from Stenian to Cambrian, with major peaks at 642 Ma and 1047 Ma (AC-05) and 634 Ma (AC-15).

Detrital zircon data from sillimanite-garnet-biotite schist (AC05) and garnet-biotite paragneiss (AC-15) indicated age spectrum between 1047 and 634 Ma with maximum age of deposition of the protoliths around 634 Ma. This result is consistent with ages of protoliths derived from magmatic arcs in the southern portion of the Pernambuco-Alagoas block north of the Brasiliano/Pan-African Sergipano Fold Belt which have ages around 630-570 Ma (Carvalho, 2005; Oliveira et al., 2014; Silva Filho et al., 2014). Carvalho (2005) and Oliveira et al. (2006, 2015) obtained on garnet-mica schists (FS-68) and quartzites (FS-89) ages ranging from 985 to 920 Ma. No zircon grains younger than 900 Ma were observed in both samples. Such ages (AC05 and AC15) suggest that rocks from the Macururé Domain were deposited before the Brasiliano orogeny.

On the other hand, Oliveira et al. (2015), also documented Paleoproterozoic grains, ranging from 2000 to 2150 Ma, which is not present on rocks of the ATC. Paleoproterozoic zircon grains might indicate an older source, which can be attributed to gneissic-migmatitic domes, such as the Jirau do Ponciano (Brito et al., 2009).

In our investigated rocks, 14 grains inherited from Meso/Neoproterozoic sources (1.0–0.92 Ga) suggest partial contribution of volcanic sources exhumed and eroded from the Cariris Velhos orogenic rocks. In the AC15 sample, most of the zircon grains present Neoproterozoic ages around 634 Ma indicating that the deposition period of the Macururé Domain was not before the Brasiliano Orogeny as previously suggested by Oliveira et al. (2006). Paleoproterozoic zircon ages were not recorded in the Araticum Complex, although they are common in the Macururé Domain (Oliveira et al., 2015, Fig. 1b).

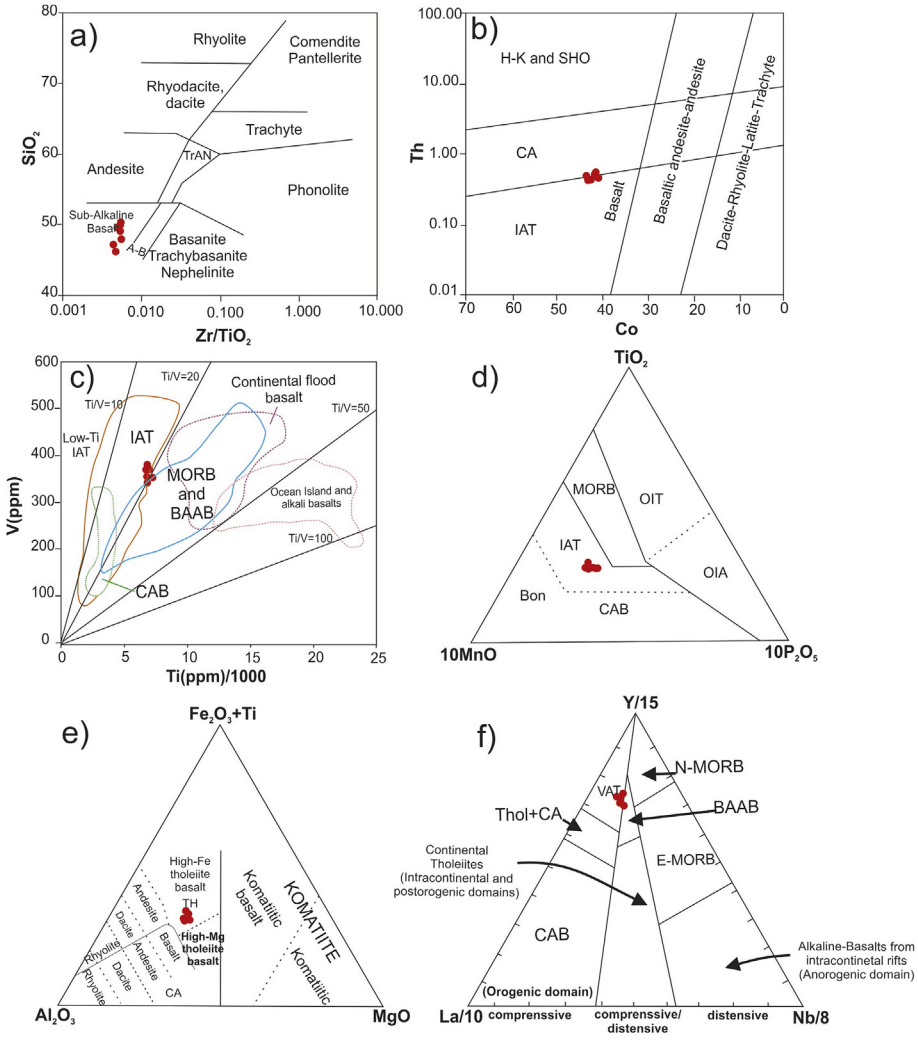

Fig. 6. Classification diagrams of volcanic rocks and tectonic environment for amphibolites of the Araticum Complex. a) Diagram of Winchester and Floyd (1977). b) Diagram of Hastie et al. (2007). c) Diagram of Shervais (1982). d) Diagram of Mullen (1983). e) Diagram of Jensen (1976) modified by Rickwood (1989). f) Diagram of Cabanis and Lecolle (1989). Abbreviations: A-B-alkaline basalt. TrAN-trachiandesite; H-K and SHO- High-K calc-alkaline and shoshonitic. CA-calc-alkaline. IAT-island arc tholeiite. CAB- calc-alkaline basalt. MORB - mid ocean ridge basalt. BAAB- back-arc basin basalts. CAB- calc-alkaline basalt. OIT - oceanic island tholeiitic basalt. Th + CA - tholeiitic and calc-alkaline basalt; VAT-volcanic arc tholeiitic basalt.

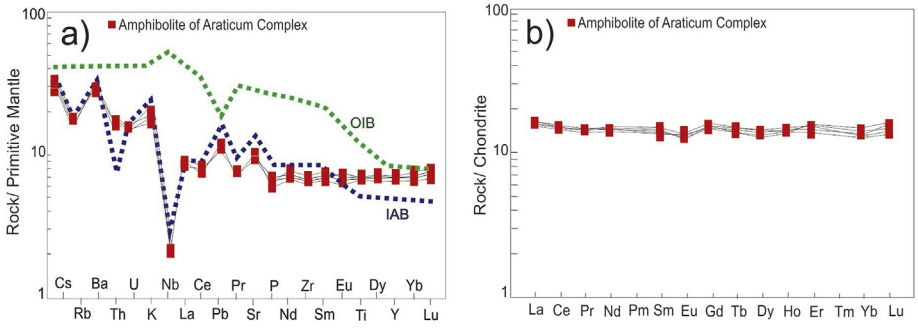

Fig. 7. A) Primitive mantle-normalized multi-element (spider) diagram for amphibolites of the Araticum Complex (Sun and McDonough, 1989 and b) Chondrite-normalized REE patterns (Sun and McDonough, 1989) for amphibolites of the Araticum Complex. OIB-oceanic island basalts and IAB- island arc basalts; values are from Sun and McDonough (1989) and Dorendorf et al. (2000).

Such results suggest that the major sources of the ATC might be associated with the Tonian Cariris Velhos orogeny, which are also described in the southern part of the Pernambuco-Alagoas Massif to the north (Silva Filho et al., 2014) and the Neoproterozoic-Cambrian Brasiliano orogen, that strongly affected the southern portion of the Borborema Province (Santos et al., 2010; Brito Neves et al., 2014; Oliveira et al., 2015). Also, very young zircon grains (Ediacaran-Cambrian) found in sample AT-05 present high Th/U ratio and might be derived from young magmatic sources, such as several unreformed post-orogenic granites that occupies the Southern portion of the Pernambuco-Alagoas Domain (Silva Filho et al., 2014).

8.3. Nd isotopes and depositional setting

The T_{DM} values of sillimanite-garnet-muscovite-biotite schists, garnet-biotite gneisses, calc-silicate rocks and marbles range between

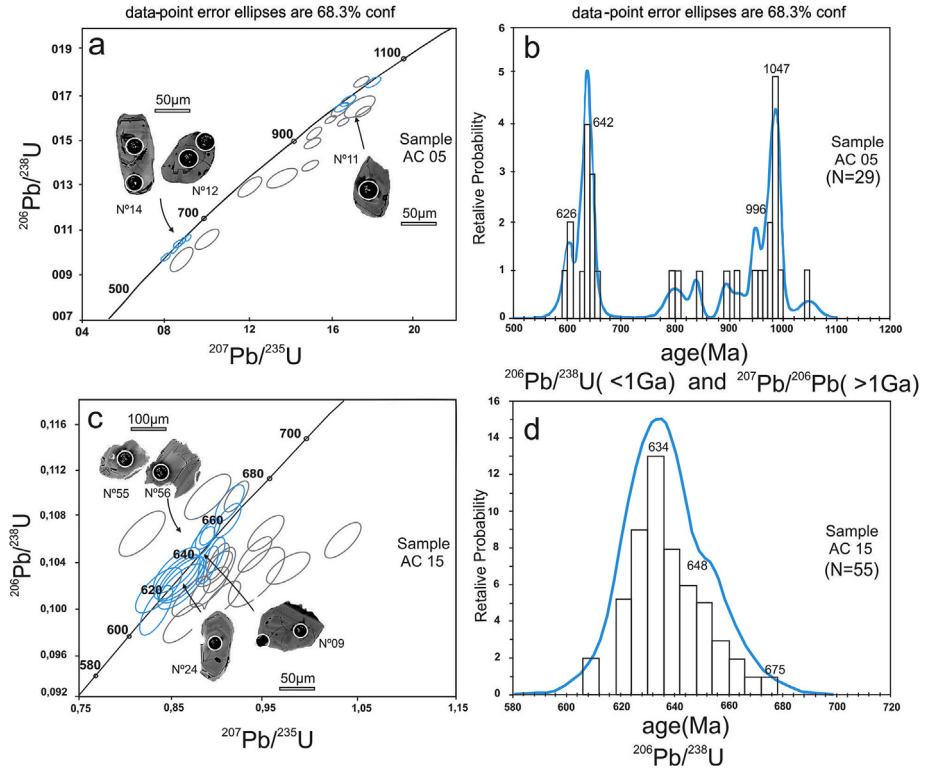

Fig. 8. Concordia diagram and histogram for Pb^{206}/U^{238} ages (best used for young zircons, ≤ca. 1000 Ma, LA-ICP-MS) ages of detrital zircon grains extracted from sillimanite-garnet-muscovite-biotite schist (AC05) and garnet-biotite paragneiss (AC15) of the Araticum Complex and their respective BSE images.

1.29 and 1.85 Ga (Table 3) indicating that the Araticum Complex has an older contribution than the Canindé (1.1–1.6 Ga), and similar to Marancó (1.18–2.23 Ga) domains. Such data also indicate that the studied sequence could be part of the Macururé Domain (1.28–1.78 Ga, Oliveira et al., 2015, Fig. 9).

According to these authors, no sample with T_{DM} ages older than 1.78 Ga was observed in the Macururé Domain. Recent regional isotopic investigations of Nd and U-Pb geochronology on detrital zircon suggest that sediments of the Marancó and Macururé domains were deposited on the continental margin of the Pernambuco-Alagoas block before the collision with the São Francisco Craton plate and that the Canindé domain probably corresponds to an aborted Neoproterozoic rift association within the southern part of the Pernambuco-Alagoas block (Oliveira et al., 2015).

According to these authors, the basal units of the Vaza-Barris and Estância domains are made of sedimentary rocks derived from the erosion of the São Francisco Craton and are interpreted as passive margin sequences with exception for Itabaiana quartzites (Vaza-Barris Domain) and Juetê diamictites (Estância Domain, Oliveira et al., 2015).

Nd isotopes and U-Pb geochronological data for detrital zircon grains in several key areas of the Sergipano Fold Belt, such as the Araticum, Arapiraca, Nicolau-Campo Grande and Jirau do Ponciano complexes are still scarce and only a few regional integration interpretations have been put forward in the last years (Carvalho, 2005; Nascimento, 2005; Oliveira et al., 2006). The geochronological pattern obtained in the present work, along with lithogeochemistry, suggests that the Araticum paleobasin was partially filled by material derived from the erosion of volcanic arcs exhumed before and during the Brasiliano/Pan-African orogeny of the Borborema Province together with some contribution from the Cariris Velhos crustal sources (1.0–0.6 Ga, Fig. 10).

Closure of the ocean, took place during successive collisional events which resulted in the construction of Ediacaran continental arcs with similar crystallization ages in the northern portion of the Sergipano Fold Belt (Canindé, Poço Redondo-Marancó and Macururé domains, 630-570 Ma (Bueno et al., 2009; Santos et al., 2004; Oliveira et al., 2010, 2015) when compared with the southern border of the Pernambuco-Alagoas Terrain (Serra do Catu, Cachoeirinhas, Águas Belas, Santana do Ipanema, Água Branca, Mata Grande and Correntes, 635-590 Ma, Silva Filho et al., 2014, 2016, Fig. 10). This collisional process is recorded by the contractional/transpressional tectonics represented by the main shear zones of the Sergipano Fold Belt developed between 650 and 540 Ma (Carvalho, 2005; Oliveira et al., 2010). We suggest as possible sources for the Araticum Complex the Neoproterozoic islands arcs (600-590Ma) that developed in the southern portion of the Pernambuco-Alagoas Domain.

These oceanic arcs were probably exhumed and eroded during the closure of the ocean with deposition of sediments on both sides of the Sergipano Fold Belt such as extensive layers of marble in the Araticum Complex.

8.4. Tectonic implications

We consider that the geotectonic model proposed by Oliveira et al. (2010, 2015) for the evolution of the Sergipano Fold Belt as the most likely. In this model the break-up of the Paleoproterozoic continent resulted in the opening of a proto-ocean on the southern coast of the Pernambuco-Alagoas block followed by subduction of oceanic

Table 5
U–Pb detrital zircon ages extracted from garnet-biotite paragneiss of the Araticum Complex.

Atomic ratios Age (Ma)												
AC15 Spot nº	$^{232}Th/^{238}U$	$^{207}Pb/^{206}Pb$	1σ (%)	$^{207}Pb/^{235}U$	1σ (%)	$^{206}Pb/^{238}U$	1σ (%)	$^{207}Pb/^{206}Pb$	1σ (%)	$^{207}Pb/^{235}U$	1σ (%)	Conc. (%)
080-ZR57	0.766	0.06030	0.82	0.890	1.30	655	12	614	35	646	12	106.7
079-ZR56	0.599	0.06158	0.80	0.884	1.23	639	10	659	34	643	12	96.8
078-ZR55	0.919	0.07062	0.87	1.030	1.28	648	11	947	35	719	13	68.5
077-ZR54	0.243	0.06131	0.78	0.880	1.27	638	11	650	33	641	12	98.2
076-ZR53	0.088	0.05994	0.61	0.854	1.07	634	10	601	26	627	10	105.5
075-ZR52	1.034	0.06191	1.03	0.866	1.55	623	13	671	44	634	15	92.8
074-ZR51	0.154	0.06085	0.67	0.880	1.09	643	9	634	29	641	10	101.5
073-ZR50	0.526	0.06214	0.91	0.885	1.45	634	13	679	39	644	14	93.4
070-ZR49	0.449	0.06372	1.02	0.900	1.49	628	12	732	43	652	14	85.8
069-ZR48	0.428	0.06192	1.16	0.890	1.61	639	13	671	49	646	15	95.2
068-ZR47	0.410	0.06269	1.03	0.871	1.56	619	13	698	44	636	15	88.8
067-ZR46	0.433	0.06306	0.66	0.904	1.07	637	9	710	28	654	10	89.7
066-ZR45	0.439	0.06131	0.90	0.869	1.43	631	13	650	38	635	13	97.0
064-ZR43	0.080	0.06411	0.59	0.900	1.20	625	12	745	25	652	11	83.8
060-ZR42	0.637	0.06465	0.78	0.951	1.17	653	10	763	33	678	12	85.6
059-ZR41	0.528	0.06239	1.05	0.878	1.49	626	12	688	45	640	14	91.1
058-ZR40	0.099	0.06235	0.67	0.883	1.10	630	9	686	29	642	10	91.8
057-ZR39	0.655	0.06486	0.73	0.937	1.17	643	10	770	31	672	11	83.5
056-ZR38	1.014	0.06342	1.24	0.889	1.68	624	13	722	52	646	16	86.4
055-ZR37B	0.560	0.06070	0.81	0.879	1.19	644	10	628	35	641	11	102.5
054-ZR37N	0.798	0.06633	1.27	0.941	2.12	631	20	817	52	673	21	77.3
053-ZR36	0.097	0.06132	0.65	0.853	1.15	620	10	650	28	626	11	95.3
049-ZR34	0.484	0.06129	1.05	0.886	1.47	643	12	650	45	644	14	99.0
048-ZR33	0.528	0.06153	0.65	0.884	1.08	639	10	658	28	643	10	97.1
047-ZR32	0.765	0.06101	0.64	0.856	1.19	625	11	640	27	628	11	97.7
046-ZR31	0.322	0.06037	0.66	0.871	1.01	642	8	617	28	636	10	104.0
045-ZR30	0.156	0.06077	0.73	0.864	1.14	633	10	631	31	632	11	100.2
044-ZR29	0.578	0.06031	0.63	0.893	1.23	658	12	632	27	648	12	107.0
040-ZR28	0.497	0.06078	0.92	0.894	1.28	653	10	691	39	648	12	103.4
039-ZR27	0.323	0.06249	0.76	0.891	1.19	634	10	647	32	647	11	91.8
038-ZR26	0.886	0.06123	1.15	0.859	1.71	625	14	618	49	630	16	96.5
037-ZR25	0.078	0.06041	0.55	0.847	0.97	624	8	633	23	623	9	101.0
036-ZR24	0.475	0.06083	0.69	0.865	1.18	632	11	775	30	633	11	99.8
035-ZR23B	0.560	0.06502	0.83	0.938	1.28	641	11	599	35	672	13	82.7
034-ZR23N	0.500	0.05986	1.49	0.837	1.98	623	15	611	64	617	18	104.0
033-ZR22	0.567	0.06021	1.37	0.853	1.97	630	16	721	59	626	18	103.1
030-ZR21	0.438	0.06337	1.07	0.863	1.58	607	13	653	45	632	15	84.3
029-ZR20B	0.103	0.06140	0.64	0.863	1.08	626	9	781	28	632	10	95.8
027-ZR19	0.596	0.06520	0.66	0.905	1.31	618	13	641	27	654	13	79.2
026-ZR18	0.593	0.06106	0.74	0.869	1.31	633	12	619	32	635	12	98.8
025-ZR17	0.338	0.06043	1.60	0.854	2.01	629	14	691	68	627	19	101.6
024-ZR16	0.538	0.06248	0.53	0.896	1.20	638	12	632	23	650	11	92.4
020-ZR15	0.317	0.06077	0.61	0.905	1.24	653	13	631	26	654	12	104.7
019-ZR14	0.432	0.06077	0.76	0.834	1.56	661	15	631	33	616	14	96.9
017-ZR12	0.590	0.06036	1.34	0.860	2.14	612	20	617	57	630	20	102.8
016-ZR11	0.337	0.06052	0.95	0.882	2.16	634	23	622	41	642	20	104.1
015-ZR10	0.353	0.06823	1.22	0.973	1.52	648	10	876	50	690	15	72.5
014-ZR9	0.120	0.06067	0.55	0.885	1.12	635	11	628	23	643	11	103.2
013-ZR8	0.357	0.05827	1.27	0.887	1.80	648	16	540	55	645	17	125.0
010-ZR7	0.150	0.06015	0.59	0.857	1.16	675	11	609	25	629	11	104.1
009-ZR6	0.640	0.06095	0.54	0.911	1.17	634	12	637	23	658	11	104.1
008-ZR5	0.498	0.06060	0.55	0.913	1.26	663	14	625	24	659	12	107.0
007-ZR4	0.647	0.06061	0.54	0.890	1.07	669	11	626	23	646	10	104.2
006-ZR3	0.897	0.06123	0.73	0.908	1.18	652	11	647	31	656	11	101.8
005-ZR2	0.505	0.06063	0.40	0.892	0.90	659	9	626	17	647	9	104.3

lithosphere and ocean closure. The extensional phase conditioned the deposition of passive margin sediments on both sides of the belt. Indications of ocean floor association were recorded in deformed pillow basalts in the Novo Gosto Unit of the Canindé Domain (Oliveira et al., 2010) and ultrabasic chlorite schists intercalated within metasedimentary rocks of the Macururé Domain (Bueno et al., 2009). Several alternative models of tectonic environment have been proposed for rocks of the Macururé Domain located in the northern portion of the Sergipano Fold Belt: deep environment (Davison and Santos, 1989), flysch sequence in continental margin (Jardim de Sá, 1992), forearc basin (Carvalho, 2005) and continental margin of the old Borborema plate before collision with the São Francisco Craton (Oliveira et al., 2015).

Brazil-Africa correlation has a major role in paleogeographic

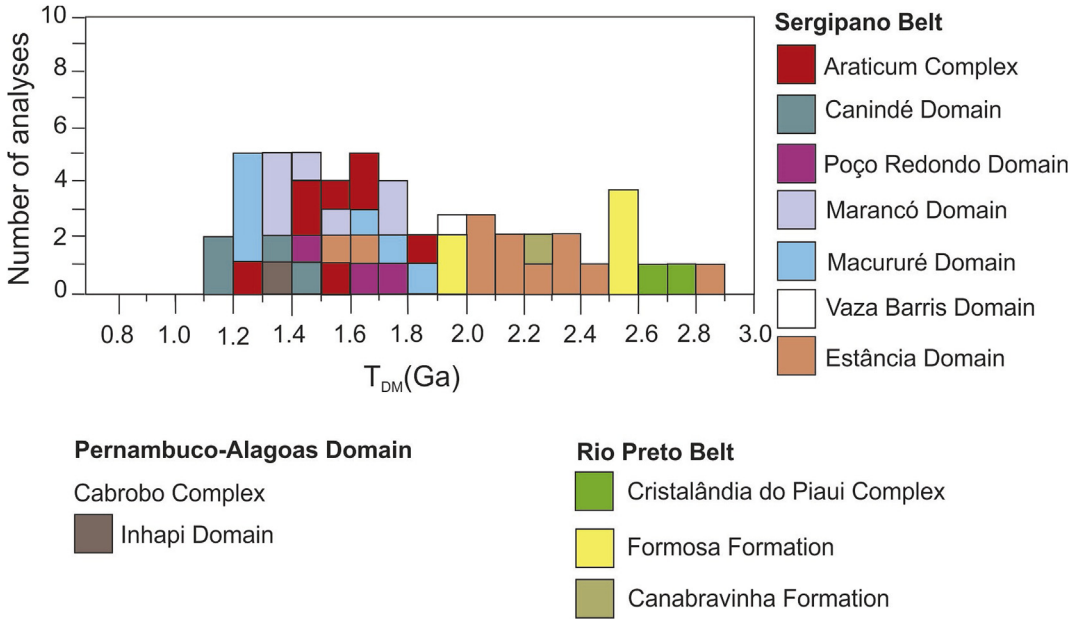

Fig. 9. Distribution of T_{DM} model ages for metasedimentary rocks of ATC-Araticum Complex compared to possible source areas of the Sergipano Fold Belt (SFB). PEAL- Pernambuco-Alagoas Domain and SFC- São Francisco Craton data from (Oliveira et al., 2010, 2015; Silva Filho et al., 2014; Caxito et al., 2014).

reconstructions of Western Gondwana, as shown by several studies (Caby, 1989; Castaing et al., 1993; Toteu et al., 2001; Brito Neves et al., 2002; Van Schmus et al., 2008). Recent lithotectonic connections between the Neoproterozoic Borborema Province in NE Brazil with West Africa domains, such as *Trans*-Saharan, Nigerian and Oubanguides mobile belts were focused on the oceanic paleobasins and proto-oceans (Van Schmus et al., 2008; Caxito et al., 2012, 2014; 2015; Alcântara et al., 2017).

In the southern sub-province of Borborema Province, in the Pernambuco-Alagoas Terrain/Massif, the isotopic data suggest that the deposition of metasedimentary sequences, generally known as the Rio Una Complex, on the Paleoproterozoic basement (Rhyacian ca. 2.2–2.0 Ga) occurred during an extensional Cryogenian event between 850 and 631 Ma (Silva Filho et al., 2014). In the Riacho do Pontal Belt the sequences of metasedimentary rocks are dominantly of Meso-Neoproterozoic ages (1.0–0.5 Ga) with a collision process similar to the Sergipano Fold Belt involving a complete tectonic cycle (Oliveira et al., 2015). Finally, in the Rio Preto Belt, Paleoproterozoic and Neoproterozoic sources, amphibolite lenses of the Formosa Formation with chemical signature of island arc environment were described by Caxito et al. (2014). The age of detrital zircon grains between 920 and 1000 Ma for sillimanite-garnet-muscovite-biotite schists (AC5, Fig. 8b) are similar the ages (980–1000 Ma) obtained for the Poço Redondo-Marancó Domain and suggests that the Cariris Velhos crust corresponds to the source region for these rocks (Carvalho, 2005; Santos et al., 2010, Fig. 1b).

Recent research by modeling has revealed that island arcs contribute more effectively to continental crust construction than continental arcs (Stern and Scholl, 2010; Jagoutz and Schmidt, 2012).

Tonian and Cryogenian to Ediacaran continental arcs are situated in the northern portion of the Sergipano Fold Belt and south of the Pernambuco-Alagoas Domain. In this context we suggest that the islands arcs and back-arc basins contributed as a source area for deposition of the Araticum complex together with of the these continental arc contribution. Therefore, the island arcs were exhumed and eroded during the subduction process during Borborema Province Neoproterozoic evolution (Fig. 10).

9. Conclusions

Our results provide new insights to understand the provenance of metasedimentary rocks in the Southern Borborema Province. Rocks that compose the Araticum metavolcanic sedimentary sequence are exposed in the NE portion of the Sergipano Fold Belt and comprises Sillimanite-garnet-biotite-muscovite schists, garnet-biotite paragneisses, metagraywackes, marbles, amphibolite and intermediate metavolcanice rocks, as well as calc-silicate rocks.

Geochemical, isotopic and geochronological data indicate that they were derived from island arc and back-arc basin settings setting involved in the collision between the São Francisco Craton and the Borborema Province. Amphibolites show positive εNd values for 900 and 600Ma suggesting juvenile sources such as island arcs. εNd (600-900Ma) values for metasedimentary rocks are also positive (1.17–10.50) indicating participation of mantle component in the source of the Araticum paleobasin. Whole rock geochemical suggest sources varying from andesites to basalts.

U-Pb zircon data indicate two different source areas associated with major peaks at ca. 642 and 1047 Ma. The maximum depositional age is interpreted as 634 Ma, which is compatible with most of granitic magmatism in the region around 600 Ma (Bueno et al., 2009; Oliveira et al., 2015), associated with collisional settings. The maximum obtained deposition age of the ATC suggest that the Marururé Domain was developed during the Brasiliano Orogeny (600 Ma), which is consistent to the model proposed by Carvalho (2005) and Oliveira et al., 2006, that suggest a possible correlation between this Domain and the Marancó Poço-Redondo Domain.

Integration of these data with available models for southern Borborema Province allow us to conclude that such orogenic complex

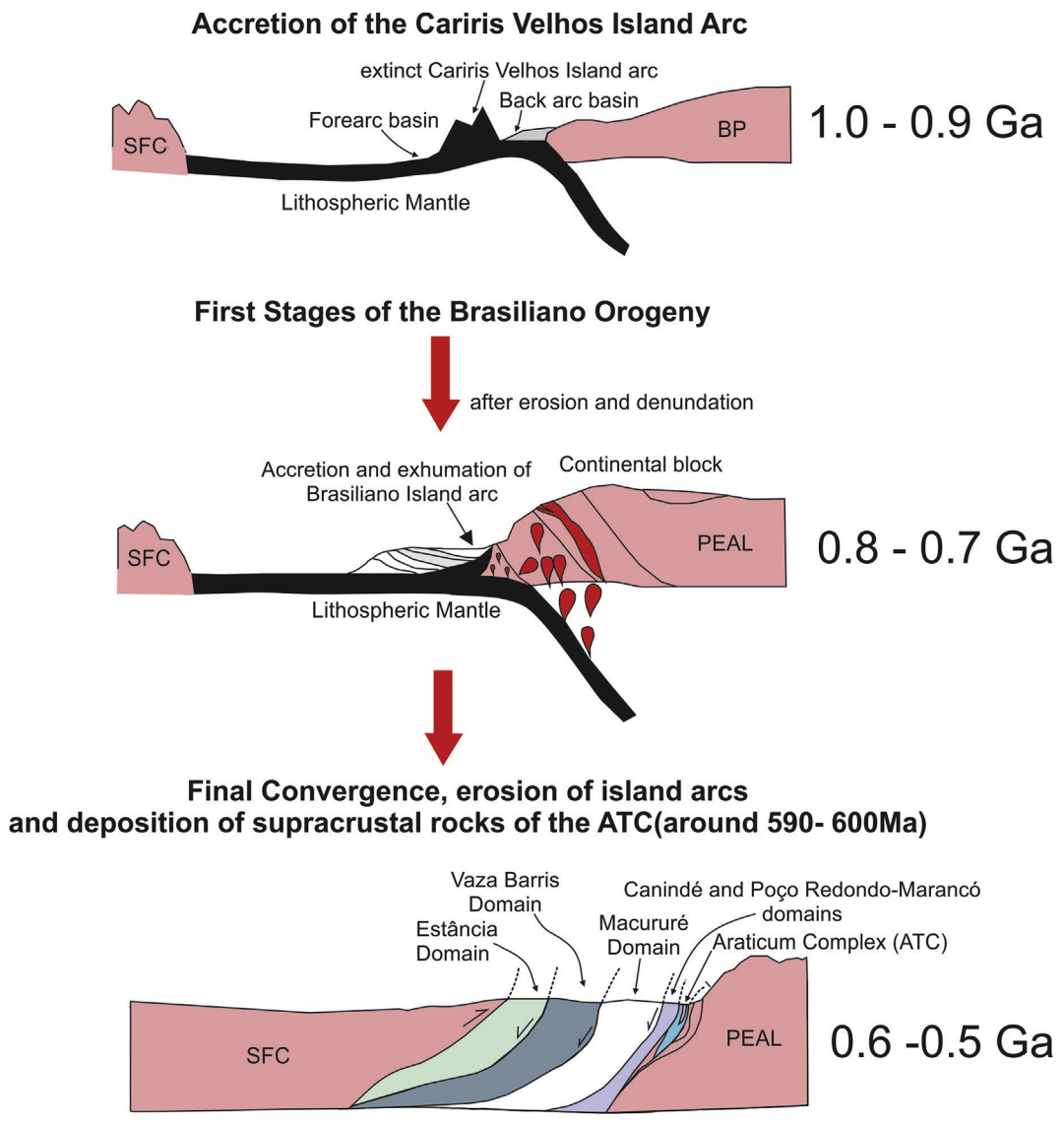

Fig. 10. Schematic picture illustrating the tectonic evolution of the northern portion of the Sergipano Belt with formation of the Araticum Complex derived from erosion of island arcs followed by the formation of continental arc around 0.6–05Ga, adjacent to the Pernambuco-Alagoas Domain.

were developed between the convergence of the Pernambuco-Alagoas Terrane and the São Francisco Craton, that was exhumed and eroded during or late in the Brasiliano-Pan-African orogeny, contributing to deposition of the Araticum sediments, coeval with several paleobasins in Western Africa such as the Lom basin in Cameroon (Toteu et al., 2006).

Acknowledgments

This work represents part of the PhD project of HML at the University of Brasília. The authors thank the financial support provided by CNPq, through grant 163462/2013-8, as well as the staff of the Geochronology Laboratory of the University of Brasília. We also express our gratitude for the two anonymous reviewers for their contribution on the original manuscript.

References

Alcântara, D.C.B.G., Uhlein, A., Caxito, F.A., Dussin, I.A., Pedrosa-Soares, A.C., 2017. Stratigraphy, tectonics and detrital zircon U-Pb (LA-ICP-MS) geochronology of the Rio Preto Belt and northern Paramirim corridor, NE, Brazil. Braz. J. Geol. 47 (2), 261–273.

Arculus, R.J., 2004. Evolution of arc magmas and their volatiles. In: In: Sparks, R.S.J., Hawkesworth, C.J. (Eds.), The State of the Planet: Frontiers and Challenges in Geophysics, Geophys. Monogr. Ser, vol. 150. pp. 95–108.

Armstrong-Altrin, J.S., Lee, Y.I., Verma, S.P., Ramasamy, S., 2004. Geochemistry of sandstones from the upper Miocene Kudankulam Formation, southern India: implications for provenance, weathering, and tectonic setting. J. Sediment. Res. 74, 285–297.

Arthaud, M.H., Caby, R., Fuck, R.A., Dantas, E.L., Parente, C.V., 2008. Geology of the Northern Borborema Province, NE Brazil and its Correlation with Nigeria, NW Africa. 294. Geological Society, London, pp. 49–67 Special Publication.

Bhatia, M.R., 1983. Plate tectonics and geochemical composition of sandstones. J. Geol. 91, 611–627.

Brito, M.F.L., Silva Filho, A.F., Guimarães, I.P., 2009. Caracterização geoquímica e isotópica do batólito Serra do Catu e sua evolução na interface dos domínios Sergipano e Per-nambuco-Alagoas, Província Borborema. Rev. Bras. Geociencias 39, 324–337.

Brito, M.F.L., Mendes, V.A., 2011. Compartimentação Tectônica da Folha Arapiraca. In: XIII Simpósio Nacional de Estudos Tectônicos e VII International Symposium on Tectonics. 286-289, Campinas, SBG.

Brito, M.F.L., Mendes, V.A., Paiva, I.P., 2008. Caracterização petrográfica e litoquímica das metamáficas do Complexo Araticum, Domínio Canindé, sistema de dobramentos sergipano, NE do Brasil. In: 44º Congresso Brasileiro de Geologia. Anais, CD-ROM, Curitiba, SBG.

Brito Neves, B.B., Van Schmus, W.R., Fetter, A.H., 2002. North-western Africa and North-eastern Brazil. Major tectonic links and correlation problems. J. Afr. Earth Sci. 34, 275–278.

Brito Neves, B.B., Santos, E.J., Van Schmus, W.R., 2000. Tectonic history of the Borborema province. In: Cordani, U.G., Milani, E.J., Thomaz Filho, A., Campos, D.A. (Eds.), Tectonic Evolution of South America. 31st International Geological Congress,

Rio de Janeiro, pp. 151–182.
Brito Neves, B.B., Fuck, R.A., Pimentel, M.M., 2014. The Brasiliano collage in South America: a review. Braz. J. Genet. 44 (3), 493–518.
Bueno, J.F., Oliveira, E.P., McNaughton, N., Laux, J.H., 2009. U–Pb dating of granites in the Neoproterozoic Sergipano Belt, NE-Brazil: implications for the timing and duration of continental collision and extrusion tectonics in the Borborema Province. Gondwana Res. 15, 86–97.
Bühn, B.M., Pimentel, M.M., Matteini, M., Dantas, E.L., 2009. High spatial resolution analysis of Pb and U isotopes for geochronology by laser ablation multicollector inductively coupled plasma mass spectrometry (LA-MC-ICP-MS). An Acad. Bras Ciências 81, 1–16.
Caby, R., 1989. Precambrian terranes of Benin-Nigeria and northeast Brazil and the late proterozoic south Atlantic fit. Geol. Soc. Am. Spec. Pap. 230, 145–158.
Cabanis, B., Lecolle, M., 1989. Le diagramme La/10-Y/15-Nb/8: un outil pour la discrimination des series volcaniques et la mise en evidence des processus de melange et/ou de contamination crustale. Comptes Rendus Academie de Sciences de Paris, Serie 2 (309), 2023–2029.
Carvalho, M.J., 2005. Evolução tectônica do Domínio Marancó – Poço Redondo: Registro das orogêneses Cariris Velhos e Brasiliana na Faixa Sergipana. Tese de Doutorado, Instituto de Geociências, Universidade Estadual de Campinas, NE Brasil, pp. 175.
Castaing, C., Triboulet, C., Feybesse, J.L., Chevremont, P., 1993. Tectonometamorphic evolution of Ghana, Togo and Benin in the light of the Pan-African/Brasiliano orogeny. Tectonophysics 218, 323–342.
Caxito, F.A., Uhlein, A., Sanglard, J.C.D., Gonçalves-Dias, T., Mendes, M.C.O., 2012. Depositional systems and stratigraphic review proposal of the Rio Preto fold belt, northwestern Bahia/southern Piauí. Rev. Bras. Geociencias 42 (3), 523–538.
Caxito, F.A., Uhlein, A., 2013. Arcabouço tectônico e estratigráfico da Faixa Riacho do Pontal, divisa Pernambuco-Piauí-Bahia. Geonomos 21 (2), 19–37.
Caxito, F.A., Dantas, E.L., Stevenson, R., Uhlein, A., 2014. Detrital zircon (U–Pb) and Sm–Nd isotope studies of the provenance and tectonic setting of basins related to collisional Orogens: the case of the Rio Preto fold belt on the northwest São Francisco Craton margin, NE Brazil. Gondwana Res. 26, 741–754.
Caxito, F.A., Uhlein, A., Dantas, E.L., Stevenson, R., Pedrosa-Soares, A.C., 2015. Orosirian (ca. 1.96 Ga) mafic crust of the northwestern São Francisco Craton margin: petrography, geochemistry and geochronology of amphibolites from the Rio Preto fold belt basement, NE Brazil. J. S. Am. Earth Sci. 59, 95–111.
Caxito, F.A., Uhlein, A., Dantas, E.L., Stevenson, R., Salgado, S.S., Dussin, I.A., Sial, A.N., 2016. A complete wilson cycle recorded within the Riacho do pontal orogen, NE Brazil: implications for the neoproterozoic evolution of the Borborema province at the heart of West Gondwana. Precambrian Res. 282, 97–120.
Cawood, P.A., Hawkesworth, C.J., Dhuime, B., 1999. Detrital zircon record and tectonic setting. Geology 40, 875–878.
Chemale Jr., F., Kawashita, K., Dussin, I.A., Ávila, J.N., Justino, D., Bertotti, A.L., 2012. U-Pb zircon in situ dating with LA-MC-ICP-MS using a mixed detector configuration. An Acad. Bras Ciências 84 (2), 275–295.
Davison, I., Santos, R.A., 1989. Tectonic evolution of the Sergipano fold belt, NE Brazil, during the Brasiliano orogeny. Precambrian Res. 45, 319–342.
D'el-Rey Silva, L.J.H., 1999. Basin infilling in the southern-central part of the Sergipano Belt, NE Brazil, and implications for the tectonic evolution of the Pan-African/Brasiliano cratons and Neoproterozoic sedimentary cover. J. S. Am. Earth Sci. 12, 453–470.
D'el-Rey Silva, L.J.H., Dantas, E.L., Teixeira, J.B.G., Laux, J.H., Silva, M.D.G., 2007. U-Pb and Sm-Nd geochronology of amphibolites from the Curaçá belt, São Francisco Cráton. Brazil. Gondwana Research 12, 454–467.
DePaolo, D.J., 1988. Neodimium Isotope Geochemistry-an Introduction. Springer-Verlag. 490p.
Dorendorf, F., Wiechert, U., Wörner, G., 2000. Hydrated sub-arc mantle: a source for the Kluchevskoy volcano, Kamchatka/Russia. Earth Planet Sci. Lett. 175, 69–86.
Fedo, C.M., Nesbitt, H.W., Young, G.M., 1995. Unraveling the effects of potassium metasomatism in sedimentary rocks and paleosols, with implications for paleo weathering conditions and provenance. Geology 23, 921–924.
Fitton, J.G., 1971. The generation of magmas in island arcs. Earth Planet Sci. Lett. 11, 63–67.
Ganade de Araujo, C.E., Rubatto, D., Hermann, J., Cordani, G.U., Caby, R., Basei, M.A.S., 2014. Ediacaran 2,500 km-long synchronous deep continental subduction in the West Gondwana Orogen. Nat. Commun. 1, 1–8.
Gioia, S.M.C.L., Pimentel, M.M., 2000. The Sm-Nd isotopic method in the geochronology laboratory of the university of Brasília. An Acad. Bras Ciências 72 (2), 219–245.
Gu, X.X., Liu, J.M., Zheng, M.H., Tang, J.X., Qi, L., 2002. Provenance and tectonic setting of the Proterozoic turbidites in Hunan, South China: geochemical evidence. J. Sediment. Res. 72, 393–407.
Haskin, L.A., Wildeman, T.R., Frey, F.A., Collins, K.A., Keedy, C.R., Haskin, M.A., 1966. Rare earths in sediments. J. Geophys. Res. B: Solid Earth 71 (24), 6091–6105.
Haskin, M.A., Haskin, L.A., 1966. Rare earths in European shales; a redetermination. Science 154, 507–509.
Hastie, A.H., Kerr, A.C., Pearce, J.A., Mitchell, S.F., 2007. Classification of altered volcanic island arc rocks using immobile trace elements: development of the Th–Co discrimination diagram. J. Petrol. 48, 2341–2357.
Hollanda, M.H.B.M., Archanjo, C.J., Batista, J.R., Souza, L.C., 2015. Detrital zircon ages and Nd isotope compositions of the Seridó and Lavras da Mangabeira basins (Borborema Province, NE Brazil): evidence for exhumation and recycling associated with a major shift in sedimentary provenance. Precambrian Res. 258, 186–207.
Jackson, S.E., Pearson, N.J., Griffin, W.L., Belousova, E.A., 2004. The application of laser ablation-inductively coupled plasma-mass spectrometry to in situ U–Pb zircon geochronology. Chem. Geol. 211, 47–69.
Jagoutz, O., Schmidt, M.W., 2012. The formation and bulk composition of modern juvenile continental crust: the Kohistan arc. Chem. Geol. 298–299, 79–96.
Janousek, V., Farrow, C.M., Erban, V., Trubac, J., 2011. Brand new Geochemical Data Toolkit (GCDkit 3.0) - is it worth upgrading and browsing documentation? (Yes!). Geologicke vyzkumy na Morave a ve Slezsku 18, 26–30.
Jardim de Sá, E.F., Macedo, M.H.F., Fuck, R.A., Kawashita, K., 1992. Terrenos proterozoicos na Província Borborema e a margem norte do Cráton São Francisco. Rev. Bras. Geociencias 22 (4), 472–480.
Jensen, L.S., 1976. A new method of classifying alkali volcanic rocks. Ontario Division Mineral. Misc. Pap. E 66 (22).
Košler, J., Fonneland, H., Sylvester, P., Turbrett, M., Pedersen, R.B., 2002. U–Pb dating of detrital zircons for sediment provenance studies: a comparison of laser ablation ICPMS and SIMS techniques. Chem. Geol. 182, 605–618.
Ludwig, K.R., 2008. Manual for Isoplot 3.7: Berkeley Geochronology Center. pp. 77 Special Publication N°. 4. rev. August 26, 2008.
Maynard, J.B., Valloni, R., Yu, H., 1982. Composition of modern deep-sea sands from arc-related basins. In: Legget, J.K. (Ed.), Trench-forearc Geology: Sedimentation and Tectonics on Modern and Ancient Active Plate Margins. vol. 10. Geological Society of London, pp. 551–561 Special Publication.
McLennan, S.M., Hemming, S., McDaniel, D.K., Hanson, G.N., 1993. Geochemical approaches to sedimentation, provenance and tectonics. In: Johnsson, M.J., Basu, A. (Eds.), Processes Controlling the Composition of Clastic Sediments. vol. 284. Geological Society of America, Boulder, CO, USA, pp. 21–40 Special Paper.
Medeiros, V.C., 2000. Aracaju NE: Folha SC.24-X estados da Paraíba, Pernambuco, Alagoas, Sergipe e Bahia. Escala 1:500.000. Brasília: CPRM, 1 CD-ROM; mapas. In: Programa Levantamentos Geológicos Básicos do Brasil - PLGB.
Mendes, V.A., Brito, M.F.L., Paiva, I.P., 2009. In: Programa Geologia do Brasil-PGB. Arapiraca. Folha SC.24-X-D. Estado de Alagoas, Pernambuco e Sergipe. Mapa Geológico. Escala: 1:250.000, Recife.
Mendes, V.A., Brito, M.F.L., Santos, C.A., 2011. Zona de Cisalhamento Contracional de Palmeira dos Índios. Um possível Testemunho do Evento Cariris Velhos na Província Borborema. In: XIII Simpósio Nacional de Estudos Tectônicos e VII International Symposium on Tectonics. SBG, Campinas, pp. 290–293.
Mullen, E.D., 1983. MnO/TiO_2, P_2O_5: a minor element discriminant for basaltic rocks of oceanic environments and its implications for petrogenesis. Earth Planet Sci. Lett. 62, 53–62.
Nascimento, R.S., 2005. Domínio Canindé, Faixa Sergipana, Nordeste do Brasil: um estudo geoquímico e isotópico de uma seqüência de rifte continental neoproterozóica. Tese de Doutorado. Programa de Pós-graduação em Geociências, Instituto de Geociências, Universidade Federal de Campinas, pp. 159.
Nesbitt, H.W., Young, G.M., 1982. Early Proterozoic climates and plate motions inferred from major element chemistry of lutites. Nature 299, 715–717.
Nesbitt, H.W., Young, G.M., McLennan, S.M., Keays, R.R., 1996. Effects of chemical weathering and sorting on petrogenesis of siliciclastic sediments, with implications for provenance studies. J. Geol. 104, 525–542.
Neves, S.P., Alcantara, V.J., 2010. Geochemistry of orthogneisses and metasedimentary rocks across a proposed terrane boundary in the Central Domain of Borborema Province, NE Brazil: geodynamic implications. J. S. Am. Earth Sci. 29, 498–511.
Neves, S.P., Bruguier, O., Silva, J.M.R., Bosch, D., Alcantara, V.C., Lima, C.M., 2009. The age distributions of detrital zircons in metasedimentary sequences in eastern Borborema Province (NE Brazil): evidence for intracontinental sedimentation and orogenesis? Precambrian Res. 175, 187–205.
Neves, S.P., Lages, G.A., Brasilino, R.G., Miranda, A.W.A., 2015. Paleoproterozoic accretionary and collisional processes and the build-up of the Borborema Province (NE Brazil): geochronological and geochemical evidence from the Central Domain. J. S. Am. Earth Sci. 58, 165–187.
Neves, S.P., Silva, J.M.R., Bruguier, O., 2017. Geometry, kinematics and geochronology of the Sertânia Complex (central Borborema Province, NE Brazil): assessing the role of accretionary versus intraplate processes during Western Gondwana assembly. Precambrian Res. 298, 552–571.
Oliveira, E.P., Toteu, S.F., Araújo, M.J., Carvalho, M.J., Nascimento, R.S., Bueno, J.F., McNaughton, N., Basilici, G., 2006. Geologic correlation between the neoproterozoic Sergipano belt (NE Brazil) and the Yaoundé belt (Cameroon, Africa). J. Afr. Earth Sci. 44, 470–478.
Oliveira, E.P., Windley, B.F., Araújo, M.N.C., 2010. The Neoproterozoic Sergipano orogenic belt, NE Brazil: a complete plate tectonic cycle in western Gondwana. Precambrian Res. 181, 64–84.
Oliveira, E.P., Bueno, J.F., McNaughton, N.J., Silva Filho, A.F., Nascimento, R.S., Donatti-Filho, J.P., 2014. Age, composition, and source of continental arc- and syn-collision granites of the neoproterozoic Sergipano belt, southern Borborema province, Brazil. J. S. Am. Earth Sci. 58, 257–280.
Oliveira, E.P., Mcnaughton, N., Windley, B.F., Carvalho, M.J., Nascimento, R.S., 2015. Detrital Zircon U-pb Geochronology and Whole-rock Nd-isotope Constraints on Sediment Provenance in the Neoproterozoic Sergipano Orogen, Brazil: from Early Passive Margins to Late Foreland Basins. Tectonophysics 662, 183–194.
Padilha, A.L., Vitorello, Í., Pádua, M.B., Fuck, R.A., 2016. Deep magnetotelluric signatures of the early neoproterozoic Cariris Velhos tectonic event within the transversal sub-province of the Borborema Province, NE Brazil. Precambrian Res. 275, 7–83.
Petrelli, M., Poli, G., Perugini, D., Peccerillo, A., 2005. PetroGraph: a new software to visualize, model, and present geochemical data in Igneous Petrology. G-cubed 6, 1–15.
Rickwood, P.C., 1989. Boundary lines within petrologic diagrams which use oxides of major and minor elements. Lithos 22, 247–263.
Roser, B.P., Korsch, R.J., 1986. Determination of tectonic setting of sandstone-mudstone suites using SiO_2 content and K_2O/Na_2O ratio. J. Geol. 94 (5), 635–650.
Roser, B.P., Korsch, R.J., 1988. Provenance signatures of sandstone-mudstone suites

determined using discrimination function analysis of major-element data. Chem. Geol. 67, 119–139.
Roser, B.P., Cooper, R.A., Nathan, S., Tulloch, A.J., 1996. Reconnaissance sandstone geochemistry, provenance, and tectonic setting of the lower Paleozoic terranes of the West Coast and Nelson, New Zealand. NZ. J. Geol. Geophys. 39, 1–16.
Rudnick, R.L., Gao, S., 2003. Composition of the continental crust. In: In: Holland, H.D., Turekian, K.K. (Eds.), Treatise on Geochemistry 3. Elsevier, Amsterdam, pp. 1–64.
Shervais, J.W., 1982. Ti–V plots and the petrogenesis of modern ophiolitic lavas. Earth Planet Sci. Lett. 59, 101–118.
Santos, L.C.M.L., Dantas, E.L., Vidotti, R.M., Cawood, P.A., Santos, E.J., Fuck, R.A., Lima, H.M., 2018a. Two-stage terrane assembly in Western Gondwana: insights from structural geology and geophysical data of central Borborema Province, NE Brazil. J. Struct. Geol. 103, 167–184.
Santos, L.C.M.L., Dantas, E.L., Cawood, P.A., Santos, E.J., Fuck, R.A., 2018b. Neoarchean crustal growth and Paleoproterozoic reworking in the Borborema Province, NE Brazil: insights from geochemical and isotopic data of TTG and metagranitic rocks of the Alto Moxotó Terrane. J. S. Am. Earth Sci. 79, 342–363.
Santos, E.J., Van Schmus, W.R., Kozuch, M., Brito Neves, B.B., 2010. The Cariris Velhos tectonic event in Northeast Brazil. J. S. Am. Earth Sci. 29, 61–76.
Santos, E.J., Nutman, A.P., Brito Neves, B.B., 2004. Idades SHRIMP U-Pb do Complexo Sertânia: implicações sobre a evolução tectônica da Zona Transversal, Província Borborema. Geol. Usp. Série Científica 4, 1–12.
Santos, E.J., 1996. Ensaio preliminar sobre terrenos e tectônica acrecionária na Província Borborema. In: SBG, Congresso Brasileiro de Geologia, 39º, Salvador. Anais 47–50.
Silva Filho, A.F., Guimarães, I.P., Van Schmus, W.R., Armstrong, R.A., Silva, J.M.R., Osako, L.S., Cocentino, L.M., 2014. SHRIMP U–Pb zircon geochronology and Nd signatures of supracrustal sequences and orthogneisses constrain the Neoproterozoic evolution of the Pernambuco–Alagoas domain, southern part of Borborema Province, NE Brazil. Int. J. Earth Sci. 103, 2155–2190.
Silva Filho, A.F., Guimarães, I.P., Santos, L., Armstrong, R., Van Schmus, W.R., 2016. Geochemistry, U-Pb geochronology, Sm-Nd and O isotopes of ca. 50 Ma long Ediacaran high-K syn-collisional magmatism in the Pernambuco alagoas domain, Borborema province, NE Brazil. J. S. Am. Earth Sci. 68, 134–154.
Silva, L.C., Pedrosa-Soares, A.C., Teixeira, L.R., Armstrong, R., 2008. Tonian rift-related, A-type continental plutonism in the Aracuaí Orogen, eastern Brazil: new evidence for the breakup stage of the São Francisco-Congo Paleocontinent. Gondwana Res. 13, 527–537.
Stern, R.J., Scholl, D.W., 2010. Yin and yang of continental crust creation and destruction by plate tectonic processes. Int. Geol. Rev. 52, 1–31.
Sun, S.S., McDonough, W.F., 1989. Chemical and isotopic systematics of oceanic basalts; implications for mantle composition and processes. In: Saunders, A.D., Norry, M.J. (Eds.), Magmatism in the Ocean Basins. Geological Society of London. vol. 42. Special Publications, London, pp. 313–345.
Taylor, S.R., McLennan, S.M., 1985. The continental Crust: its Composition and Evolution. Oxford, Blackwell, pp. 312.
Toteu, S.F., Van Schmus, W.R., Penaye, J., Michard, A., 2001. New U-Pb and Sm-Nd data from north-central Cameroon and its bearing on the pre-Pan African history of Central Africa. Precambrian Res. 108, 45–73.
Toteu, S.F., Penaye, J., Deloule, E., Van Schmus, W.R., Tchameni, R., 2006. Diachronous evolution of volcano-sedimentary basins north of the Congo craton: insights from U–Pb ion microprobe dating of zircons from the Poli, Lom and Yaoundé Groups (Cameroon). J. Afr. Earth Sci. 44, 428–442.
Trompette, R., 1994. Geology of Western Gondwana (2000-500 Ma). Balkema, Rotterdam, pp. 350.
Ulmer, P., 2001. Partial melting in the mantle wedge the role of H_2O in the genesis of mantle-derived 'arc-related' magmas. Phys. Earth Planet. In. 127, 215–232.
Van Schmus, W.R., Brito Neves, B.B., Hackspacher, P., Babinski, M., 1995. U/Pb and Sm/Nd geochronologic studies of eastern Borborema Province, northeastern Brazil: initial conclusions. J. S. Am. Earth Sci. 8, 267–288.
Van Schmus, W.R., Oliveira, E.P., Silva Filho, A.F., Toteu, F., Penaye, J., Guimarães, I.P., 2008. Proterozoic links between the Borborema province, NE Brazil, and the central African fold belt, vol. 294. Geological Society, London, pp. 66–69 Special Publications.
Van Schmus, W.R., Kozuch, M., Brito Neves, B.B., 2011. Precambrian history of the zona transversal of the Borborema province, NE Brazil: insights from Sm-Nd and U-Pb geochronology. J. S. Am. Earth Sci. 31 (2), 227–252.
Winchester, J.A., Floyd, P.A., 1977. Geochemical discrimination of different magma series and their differentiation products using immobile elements. Chem. Geol. 20, 325–343.